LIM-Nebulette Reinforces Podocyte Structural Integrity by Linking Actin and Vimentin Filaments

Xuhua Ge ,[1] Tao Zhang ,[1] Xiaoxia Yu ,[1] Alecia N. Muwonge ,[1]
Nanditha Anandakrishnan ,[1] Nicholas J. Wong ,[1] Jonathan C. Haydak ,[1]
Jordan M. Reid ,[1] Jia Fu ,[1] Jenny S. Wong ,[1] Smiti Bhattacharya ,[1,2]
Christina M. Cuttitta,[1] Fang Zhong,[1] Ronald E. Gordon,[3] Fadi Salem ,[3] William Janssen,[4]
James C. Hone ,[2] Aihua Zhang ,[5] Hong Li ,[6] John C. He ,[1,7] G. Luca Gusella ,[1]
Kirk N. Campbell ,[1] and Evren U. Azeloglu [1,7]

Due to the number of contributing authors, the affiliations are listed at the end of this article.

ABSTRACT

Background Maintenance of the intricate interdigitating morphology of podocytes is crucial for glomerular filtration. One of the key aspects of specialized podocyte morphology is the segregation and organization of distinct cytoskeletal filaments into different subcellular components, for which the exact mechanisms remain poorly understood.

Methods Cells from rats, mice, and humans were used to describe the cytoskeletal configuration underlying podocyte structure. Screening the time-dependent proteomic changes in the rat puromycin aminonucleoside–induced nephropathy model correlated the actin-binding protein LIM-nebulette strongly with glomerular function. Single-cell RNA sequencing and immunogold labeling were used to determine *Nebl* expression specificity in podocytes. Automated high-content imaging, super-resolution microscopy, atomic force microscopy (AFM), live-cell imaging of calcium, and measurement of motility and adhesion dynamics characterized the physiologic role of LIM-nebulette in podocytes.

Results *Nebl* knockout mice have increased susceptibility to adriamycin-induced nephropathy and display morphologic, cytoskeletal, and focal adhesion abnormalities with altered calcium dynamics, motility, and Rho GTPase activity. LIM-nebulette expression is decreased in diabetic nephropathy and FSGS patients at both the transcript and protein level. In mice, rats, and humans, LIM-nebulette expression is localized to primary, secondary, and tertiary processes of podocytes, where it colocalizes with focal adhesions as well as with vimentin fibers. LIM-nebulette shRNA knockdown in immortalized human podocytes leads to dysregulation of vimentin filament organization and reduced cellular elasticity as measured by AFM indentation.

Conclusions LIM-nebulette is a multifunctional cytoskeletal protein that is critical in the maintenance of podocyte structural integrity through active reorganization of focal adhesions, the actin cytoskeleton, and intermediate filaments.

Podocytes perform a critical structural role in formation and maintenance of the glomerular filtration barrier, and operate in a physically demanding microenvironment, whereby mechanical challenges, such as shear stress, seriously affect their homeostasis.[1,2] Accordingly, biomechanical properties of podocytes are central for carrying out their

physiologic function.[3,4] Alterations in podocyte biomechanics have been linked to numerous glomerular disease conditions[5] as well as drug-induced glomerular adverse events.[6] A number of podocyte-specific proteins have been associated with the loss of appropriate biomechanical microenvironment that leads to glomerular dysfunction and nephropathy[7–9]; these proteins are often associated with the structural or adhesive machinery of the podocyte that allows the maintenance of their intricate three-dimensional morphology through a highly specialized cytoskeletal backbone.[10]

The podocyte cytoskeleton has been implicated as a key player in adaptation of its cellular biomechanics to altered biophysical cues during health and disease. However, the main focus of this research has mostly been the actin cytoskeleton[11]; very little is known about the role of other cytoskeletal components, such as intermediate filaments, in podocyte biology. Intermediate filaments, such as vimentin and desmin, play a structural role in stabilizing cellular biomechanics.[12] They are ubiquitously expressed throughout the cell body of kidney podocytes, and they are thought to play a role in formation and maintenance of primary processes[13] and their structural stability.[14] The changes in the expression signature of intermediate filaments in podocytes have been associated with pathophysiologic changes, such as the differentiation state of cells during disease conditions.[15,16] However, how intermediate filaments are linked to the rest of the specialized podocyte cytoskeletal machinery remains elusive.[17]

Here, we show that LIM-nebulette, an actin-associated protein with multiple protein-binding domains,[18] may play a key role in bridging vimentin to the crosslinked actin stress fibers, thereby increasing their biomechanical stability. Using multiple omics approaches, we show that LIM-nebulette is specific to the kidney podocyte within the glomerulus. We further use an integrative approach to demonstrate that LIM-nebulette plays a multifaceted role in physiologic function of the podocyte, including the maintenance of the healthy foot process morphology *in vivo*, and that its downregulation is associated with glomerular disease in humans.

METHODS

Animal Studies

Animals received humane and ethical treatment as outlined by the National Institutes of Health (NIH) Guide for the Care and Use of Laboratory Animals.[19] All animal studies were reviewed and approved by the Institutional Animal Care and Use Committee in Icahn School of Medicine at Mount Sinai.

Rats

Male Sprague Dawley rats (6–8 weeks old) were treated with puromycin aminonucleoside (PAN) (catalog #P7130, 100 mg/kg; Sigma Aldrich) through a single tail-vein injection. Weights and urine samples were collected before the rats were euthanized. Half of the rats were used for RNA/protein

Significance Statement

The functional basis of the spatial cytoskeletal organization in the kidney podocyte that gives rise to its unique interdigitating morphology has been elusive. An integrative approach identified a novel podocyte-specific actin-associated protein, LIM-nebulette, that brings vimentin intermediate filaments to actin microfilaments, promoting mechanical stability, by regulating focal adhesions, calcium dynamics, and Rho GTPase activity. Silencing of LIM-nebulette is associated with aberrant biophysical properties in human podocytes in culture as well as with multiple glomerulopathies in patients, at both the RNA transcript and protein levels.

isolation, whereas the other half were used for histopathology and electron microscopy. For the former, kidneys were harvested after perfusion with cold PBS and glomeruli were isolated by sieving through 75/150/200 steel meshes, as previously described.[20] For the latter, animals were perfused with cold PBS followed by 4% paraformaldehyde (PFA) in PBS. Small cortical pieces were dissected and postfixed with 2.5% glutaraldehyde in sodium cacodylic buffer for transmission electron microscopy (TEM).

Mice

$Nebl^{+/+}$ wild-type (WT) and $Nebl^{-/-}$ knockout (KO) littermates of mixed C57BL/6 mice (7–8 weeks old) were randomly assigned to PBS (vehicle) or adriamycin (ADR) challenge groups. Both WT and KO groups were treated with ADR (15 mg per kg body wt, catalog #NDC 0069–3032–20; Pfizer) or vehicle (PBS) by single tail-vein injection. In addition to baseline, urine was collected from these mice at weeks 1, 2, 3, and 4 after injection. Four weeks postinjection, blood was collected from the inferior vena cava, and the kidneys were harvested after perfusion with cold PBS followed by cold 3% PFA in PBS at pH 7.4–7.6.

For primary podocyte culture from $Nebl^{+/+}$ and $Nebl^{-/-}$ mice, animals were anesthetized with intraperitoneal ketamine/xylazine and subsequently immobilized once deep anesthesia was confirmed. They were each perfused through the left ventricle with approximately 60 ml of a solution containing 2.5 mg/ml iron oxide (catalog #310050; Sigma Aldrich) and 1% BSA (catalog #A9430; Sigma Aldrich) in 1× HBSS (catalog #14025–092; Life Technologies). Both kidneys were removed, pulverized, then transferred to a 2-ml microcentrifuge tube containing 1× HBSS, 10 mg/ml Collagenase A (catalog #10103578001; Roche), and 1000 U/ml DNase I (catalog #D4513; Sigma Aldrich). After rotating the minced kidney at 37°C for 30 minutes to digest the tissue, the sample was passed through a 100-μm strainer and washed with cold 1× HBSS. It was then passed through a second 100-μm strainer. The collected sample was centrifuged for 5 minutes at 200 × g at 4°C. The iron-bounded glomeruli were recovered, resuspended in 1× HBSS, and then immediately transferred to a new 2-ml microcentrifuge tube, which was placed on a magnetic concentrator on ice. The supernatant and the excess tissue were carefully removed with a 1-ml pipette. The iron-bound

glomeruli were washed repeatedly with 1× HBSS until a pure suspension of glomeruli without tubules was detected under a microscope.

Isobaric-Tagged Proteomics

Quantitative shotgun proteomics was performed as previously described.[20] Briefly, samples were lysed with sonication in 8 M urea with 100 mM triethylammonium bicarbonate and 1% octyl-beta-D-glucopyranoside supplemented with protease and phosphatase inhibitors. After clearing the supernatant by high-speed centrifugation for 15 minutes, lysates were transferred to new 1.5-ml tubes and reduced with Tris(2-carboxyethyl)-phosphine. After blocking free thiols with methanethiosulfonate, proteins were digested with Lys-C for 4 hours and with trypsin overnight, both at 37°C. Peptides were then labeled with iTRAQ tags (AB Sciex) per manufacturer's instructions and dried overnight. The iTRAQ-labeled peptides were mixed together and then fractionated *via* strong cation exchange chromatography and desalted with C_{18} spin columns.[21,22] Liquid chromatography with tandem mass spectrometry (LC-MS/MS) was performed on an UltiMate 3000 nano LC system (Dionex) and LTQ Orbitrap Velos mass spectrometer (Thermo). The MS/MS spectra were searched against the rat SwissProt proteome using Mascot and SEQUEST search engines *via* the Proteome Discoverer platform (Thermo Scientific). A false peptide discovery rate of 1% with a minimum of two peptides per protein was used as the identification threshold. Normalized protein-level iTRAQ ratios were used for quantification.

Urine Albumin–Creatinine Assay

Urine albumin was quantified by an ELISA according to the manufacturer's instructions (catalog #E111–125; Bethyl Laboratories). Urine creatinine levels were also quantified in these samples using creatinine colorimetric assay reagents (catalog #500701; Cayman Chemicals), also according to the manufacturer's instructions. The urine albumin excretion rate was expressed as the ratio of albumin to creatinine.

Single-Cell RNA Sequencing

A single-cell suspension of dissociated mouse glomerular cells was freshly isolated from 12 18-week-old mice in C57BL/6 background as previously reported.[23] Briefly, cells were suspended in the buffer for separation using the Fluidigm C1 Single-Cell Auto Prep System (Fluidigm Corporation) and loaded onto the 800-cell (version 2) integrated fluidic circuits following the manufacturer's instructions. The final pooled libraries from each experiment were sequenced on an Illumina NextSeq 500 platform in the Genomics Core Facility of The Rockefeller University. After the QC filters, a total of 326 cells from two independent experiments were analyzed with a median of 3417 genes per cell at a sequencing depth of approximately 40,000 aligned reads per cell. Uniform Manifold Approximation and Projection dimensional reduction was performed and cells were clustered using *FindClusters*

function with *resolution*=0.7. Each cluster was screened for marker genes by differential expression analysis between cells inside and outside of the cluster using *FindMarkers* function with parameters min.pct=0.25 (genes expressed in at least 25% of cells either inside or outside of a cluster) and test.use="wilcox" (Wilcoxon rank sum test).

Quantitative RT-PCR

Cellular RNA was extracted using TRIzol reagent (catalog #15596026; Invitrogen). First-strand cDNA was reverse-transcribed from a total of 1 μg of RNA using the SuperScript III First-Strand Synthesis System (catalog #18080051; Invitrogen). A total of 1 μg of cDNA was amplified in a 20-μl reaction system containing 10 μl of Power SYBR Green PCR Master Mix (catalog #4367659; Thermo Fisher Scientific) and 400 nmol/L primer mixture. All of the primers used for this process are denoted in Supplemental Table 1. Because the two isoforms of the *Nebl* gene produce two distinct proteins, isoform specificity was observed wherever appropriate. Glyceraldehyde-3-phosphate dehydrogenase was used as an internal loading control. The $2^{-\Delta\Delta Ct}$ method was used for the analysis of relative gene expression.

Primary Mouse Podocyte Cell Culture

Isolated glomeruli were resuspended in RPMI-based mouse podocyte growth media with 10% FBS (catalog #26140–079; Thermo Fisher), transferred to collagen-coated cell culture flasks, and incubated at 33°C for 5–7 consecutive days without disturbance. After this period, the flask was observed under a microscope to detect adherence of glomeruli and appearance of primary mouse podocytes on the surface of the flask. Cells were then trypsinized with 0.05% trypsin EDTA (catalog #25300–054; Thermo Fisher), and strained with a 40-μm cell strainer (catalog #352340; Thermo Fisher) to remove tissue and cellular debris. Podocytes were then washed with mouse podocyte cell growth medium, centrifuged, and subcultured onto sterile #1.5 round 12-mm or 25-mm glass coverslips, which were incubated at 37°C for 2 days before the experiments. Thereafter, the podocytes were processed for future analyses.

Stable Knockdown and Overexpression of LIM-Nebulette in Human Podocytes

HEK293T cells, which were used for generation of viral plasmids, were cultured in 10% FBS in DMEM (catalog #670087; Life Technologies). Lentiviral vectors, expressing either scrambled shRNA or nebulette shRNA (catalog #TL302993; OriGene Technologies) and myc-tagged LIM-nebulette (catalog #RC212733, NM_213569; OriGene Technologies), were produced by cotransfecting HEK293T cells with psPAX2 packaging plasmid (catalog #12260; Addgene) and pMD2.G envelope plasmid (catalog #12259; Addgene) using Lipofectamine 3000 Transfection Kit (catalog #L3000–015, Lot# 1857479; Invitrogen) according to the manufacturer's instructions. For transduction of immortalized human podocytes, cells

were incubated with viral supernatants supplemented with 3–4 μg/ml polybrene at 33°C for 24 hours, followed by puromycin selection for an additional 72 hours. All human podocyte cell line experiments were carried out after 10–14 days of thermoshifted 37°C culture.

Differentiated human immortalized podocytes were treated with various cytoskeletal toxins to understand the effect of cytoskeletal disruption on the translocation and subcellular localization of LIM-nebulette. The following cytoskeletal disruptors were used for F-actin: 0.5 μM Cytochalasin D (catalog #C8273; Sigma) for 1 hour and 0.1 μM Latrunculin B (catalog #10010631; Cayman Chemical) for 1 hour. For targeting vimentin, 10 μM Arylquin-1 (catalog #16961; Cayman Chemical) for 1 hour and 10 μM Withaferin A (catalog #11352; Cayman Chemical) for 18 hours were used. After treatment with the inhibitors, the cells were fixed, immunostained, and imaged on a Zeiss LSM 880 super-resolution laser scanning confocal microscope with Airyscan using a 63× 1.4 NA oil immersion lens.

G-LISA Small GTPase Activity Assay

Innate activity of the small molecule RhoA GTPase was measured using the colorimetric G-LISA small G-protein activation assay (catalog #BK135; Cytoskeleton Inc.) per the manufacturer's protocol. Briefly, WT ($Nebl^{+/+}$) and KO ($Nebl^{-/-}$) mice were perfused with iron oxide, the kidneys were removed, and the glomeruli were isolated as previously described.[24] The isolated glomeruli were lysed using a buffer containing Tris, $MgCl_2$, NaCl, IGEPAL, SDS (GL36), and protease inhibitor cocktail, and immediately flash-frozen in liquid nitrogen. After completion of all tissue collection and lysis, protein lysates were then used for RhoA activation detection in concentrations of 0.25–1 mg/ml. Thawed lysates, positive control, and negative control (lysis buffer blanks) were added to reaction wells in triplicates and incubated at 4°C on an orbital shaker for 30 minutes. Antigen-presenting buffer and primary and HRP-conjugated secondary antibodies were added in sequence. HRP detection reagent was then added to each reaction well and incubated for 15 minutes at 37°C. HRP stop solution was added to each well and colorimetric change was detected on a spectrophotometer (1420 Multilabel Counter VICTOR 3; Perkin Elmer) at a wavelength of 490 nm. OD values were used to assess the level of activation of RhoA in $Nebl^{+/+}$ and $Nebl^{-/-}$ glomeruli.

Directed Differentiation of human induced pluripotent stem cells

We used the previously established human induced pluripotent stem cells (hiPSCs) that were generated for the NIH LINCS consortium.[25] Cells were reprogrammed from healthy donors' skin tissue using CytoTune-iPS 2.0 Sendai Reprogramming reagents (catalog #A16518; Thermo Fisher) by the Mount Sinai Stem Cell Core Facility following the standard protocol as previously described.[26] Directed podocyte differentiation was carried out for 21 days using Wnt signaling

modulation followed by retinoic acid stimulation as previously described.[27] Divergent from the originally reported protocol, hiPSC-derived podocytes were incubated in DMEM/F12 (catalog #11320033; Thermo Fisher) with 1× insulin-transferrin-selenium (catalog #41400045; Thermo Fisher) and B-27 (catalog #17504044; Thermo Fisher) for another 9 days at 37°C, at which point all cells were quiescent. The culture medium was refreshed every third day.

Immunofluorescence Staining
Cells/Frozen Tissues
Archival deidentified human biopsy specimens of healthy cortex from clinically indicated nephrectomized patients as well as those with diabetic nephropathy (DN) or FSGS were collected at Mount Sinai Hospital, Icahn School of Medicine at Mount Sinai, New York, under a protocol approved by the Institutional Review Board. Thin sections from human kidney biopsy samples were prepared accordingly. Differentiated immortalized human podocytes were cultured on collagen-coated glass coverslips. Cells were fixed with 4% PFA in 1× PBS at room temperature for 20 minutes then treated with 0.05% Triton-X (catalog #T8787; Sigma Aldrich) permeabilization solution for 12 minutes at room temperature. The permeabilization solution was replaced with 10% blocking buffer and incubated at room temperature for 2 hours. Immunostaining was performed using the primary antibodies rabbit anti-vimentin (catalog #5741S; Cell signaling), mouse anti-synaptopodin (catalog #65294; Progen), goat anti–LIM-nebulette (catalog #NBP1–45223, Isoform-2; Novus Biologicals), mouse anti-paxillin (catalog #ma5–13356; Invitrogen), and rabbit anti–actinin-4 (catalog #ab108198; Abcam). Thereafter, sections were incubated with fluorophore-linked secondary antibodies (catalog #A11055, Alexa Fluor 488 anti-goat IgG; catalog #A10042, 568 anti-rabbit IgG; and catalog #A31571, 647 anti-mouse IgG; all from Thermo Fisher). After another wash, either AlexaFluor-568 phalloidin (when performing four-color staining, catalog #A12380) or AlexaFluor-750 phalloidin (when performing five-color staining, catalog #A30105) and Hoechst 33342 (catalog #62249; all from Thermo Fisher) were used to label F-actin and nuclei, respectively. After staining, slides were mounted in ProLong Diamond antifade mountant (catalog #P36961; Thermo Fisher).

Formalin-Fixed Paraffin-Embedded Tissues
Slides containing paraffin-embedded tissue samples were heated tissue-side-up in a microwave at high power for approximately 2 minutes. Once the paraffin had dissolved, the slides were placed in a slide rack and immersed in succession in histologic-grade xylene (catalog #X3P; Fisher Scientific) followed by decreasing concentrations of 100%, 90%, 80%, 70%, 50%, and 30% ethanol (catalog #04355226; Fisher Scientific); deionized water; and then 1× PBS. The rack containing the slides was then placed into a vegetable steamer containing preheated 10 mM citrate buffer (catalog #A104,

citric acid; Fisher Scientific; catalog #S1804, H_2O, sodium citrate; Sigma Aldrich) and boiled for 15 minutes at 100°C for antigen retrieval. After room-temperature cooling for approximately 60–90 minutes, the slides were washed with deionized water followed by 1× PBS, each for 5 minutes. Histopathologic analysis using periodic acid–Schiff, hematoxylin and eosin, Masson's trichrome, and Picrosirius red staining were performed per standardized protocols as previously described.[28,29]

Immunohistochemistry

Slides with formalin-fixed and paraffin-embedded tissue sections were initially baked for 20 minutes in a 55–60°C oven. They were then deparaffinized as described in the section above and endogenous peroxidase was inactivated with hydrogen peroxide. Sections were then blocked in 2% donkey serum in PBS for 1 hour at room temperature followed by incubation with a rabbit anti-WT1 antibody (catalog #NBP2–67587; Novus Biologicals) at 4°C overnight. The sections were then washed three times with 1× PBS solution, followed by incubation with secondary detection using discovery OmniMap anti-rabbit peroxidase (Roche Diagnostics) with a fixed exposure time for all experiments among the groups. Nuclei were counterstained with hematoxylin. The negative control consisted of a tissue section stained only with secondary antibody.

Microscopy

Different imaging techniques, including widefield, laser scanning confocal, super-resolution optical, transmission electron, and atomic force microscopy (AFM), were used in order to optimize quantitative and unbiased assessment of cell biologic or physiologic roles of LIM-nebulette. Detailed experimental protocols for these techniques and the respective analysis methods are outlined below.

Quantitative and High-Content Image Analysis

All images were systematically processed in an unbiased, blinded, semiautomated manner and quantitatively analyzed following the high-content image analysis (HCA) guidelines outlined previously.[6] For HCA of focal adhesion morphometrics, total internal reflectance fluorescence (TIRF) microscopy; for HCA of filamentous textures and measurement of calcium dynamics, laser scanning confocal microscopy; for quantification of *in vivo* foot process widths, TEM; and for HCA of immunofluorescence-based cellular and nuclear morphometrics, immunohistochemistry-based *in vivo* glomerular geometry and live-cell basal motility widefield optical microscopy have been used. For all assays, images were loaded onto ImageJ FIJI software (NIH, Bethesda, MD, rsb.info.nih.gov) and converted to 8-bit grayscale. For *in vivo* glomerular morphometrics, regions excluding the Bowman's capsule were semimanually selected for measurement of glomerular area and automatically selected and segmented for nuclear metrics. A blinded human observer confirmed all automated morphologic segmentations for all HCA assays. All other

computational assay details have been disclosed before[6]; these and additional annotated HCA scripts with protocol details can be found in the Azeloglu Lab GitHub page (https://github.com/AzelogluLab).

TIRF Microscopy

TIRF microscopy was performed using a Leica DMi8 Infinity TIRF microscope and LASX (v.3.6). Focal adhesion morphometrics were assessed using immunofluorescence staining of paxillin (at an imaging depth of 90 nm) and α-actinin-4 (at an imaging depth of 250 nm), both of which were imaged under PBS supplemented with ProLong Live antifade agent (catalog #P36975; Thermo Fisher) using a 1.4 NA Leica 63× oil TIRF objective at 30°C.

Laser Scanning Confocal Microscopy with Airyscan Super-Resolution

Laser scanning confocal microscopy was carried out using a Zeiss LSM 880 with the Airyscan Super-Resolution module with the pinhole at 1 Airy unit. For quantitative HCA, images were acquired at 2048×2048 line resolution without any binning or cropping using a 0.8 NA Zeiss 20× air objective at room temperature. High-resolution representative images were acquired using a 1.4 NA Zeiss 63× oil objective with z-sections at 150% of the optimal lateral resolution through the thickness of the samples; maximum intensity projections are presented as representative images. Laser power, gain settings, magnification, zoom, pixel size, slice thickness (for z-stacks) were held constant across all samples used during HCA imaging.

Stimulated Emission-Depletion Super-Resolution Microscopy

Stimulated emission-depletion (STED) microscopy was performed using a Leica SP8 laser scanning confocal system equipped with white-light laser and STED modules. Frozen human tissue sections were immunostained with goat anti–LIM-nebulette (catalog #NBP1–45223; Novus) and rabbit anti–actinin-4 (catalog #ab108198; Abcam) primary antibodies followed by anti–goat-Alexa Fluor 594 and anti–rabbit-Alexa Fluor 647 secondary antibodies, and imaged using a 1.4 NA Leica 100× oil objective.

Quantitative TEM

Quantitative TEM was carried out as previously described.[20] Briefly, perfused kidney tissue samples were prepared by secondary fixation with 1.5% glutaraldehyde in 0.2 M sodium cacodylic buffer followed by osmication and serial dehydration. They were then stained using uranyl acetate–lead citrate and embedded in epon resin, and ultrathin sections were cut at 80 nm. Images were captured using a Hitachi H7600 TEM at 80 kV with magnifications of ×2000 (used for quantification of foot process width) to ×10,000 (used for close evaluation of slit diaphragm status). Mean foot process width was calculated by a blinded expert tracing the capillary distance and recording the number of processes

in five glomeruli from at least two separate thin sections from each animal using FIJI.

Postembedding Immunogold Staining and Imaging
The freeze substitution and low-temperature embedding of the specimens were performed as described previously with several modifications.[30] Briefly, sections were cryoprotected by immersion in 4% D-glucose, followed by incubations of increasing concentrations of glycerol in PBS (10%, 20%, and 30%), and were moved rapidly into −180°C liquid propane cooled by liquid nitrogen in a universal cryofixation system KF80 (Reichert-Jung, Vienna, Austria). The samples were immersed in 1.5% uranyl acetate (for *en bloc* fixation) prepared in anhydrous methanol (−90°C) for 24 hours in a cryosubstitution automated freeze substitution unit (Leica, Vienna, Austria). The temperature was increased in steps of 4°C/h from −90°C to −45°C. The samples were then washed with anhydrous methanol and infiltrated with Lowicryl HM20 resin (Electron Microscopy Sciences, Fort Washington, PA) at −45°C, with a progressive increase in the ratio of resin to methanol for 1 hour each, followed with pure Lowicryl overnight. Polymerization was performed with 360-nm ultraviolet light at −45°C for 48 hours, followed by 24 hours at room temperature. Ultrathin sections were cut on a Reichert-Jung ultramicrotome (Vienna, Austria) and collected on nickel mesh grids. Grids containing the ultrathin sections were initially treated with a saturated solution of sodium hydroxide in 100% ethanol, rinsed, and treated in 0.1% sodium borohydrate and 50 mM glycine for 5 minutes, followed by treatment in Tris-buffered saline containing 2% normal human serum for 10 minutes. The immunogold procedure was carried out by incubating ultrathin sections in primary goat anti–LIM-nebulette (Isoform-2, catalog #NBP1–45223) antibody overnight followed by anti-goat 10-nm gold–conjugated secondary antibody (Electron Microscopy Sciences). Ultrathin sections were then counterstained with uranyl acetate and Reynolds lead citrate and viewed at 100 kV on a Hitachi 7700 TEM. Images were captured on an Advantage CCD camera (Advanced Microscopy Techniques Corporation, Danvers, MA). Secondary antibody specificity was established by verifying that no immunogold labeling was observed when the primary antisera were omitted from the immunocytochemical protocol.

AFM Indentation
Cellular biomechanics were assessed using AFM indentation as previously described.[31] Briefly, immortalized human podocytes were cultured at a density of 5000 per cm^2 on type I collagen–coated 50-mm low-profile culture dishes. After differentiating for 10–14 days at 37°C, dishes were transferred to an Asylum MFP3D atomic force microscope enclosed in an environmentally controlled vibration isolation chamber. All experiments were carried out at 37°C with regular culture medium. Scrambled or shRNA cells were probed over a 20-μm^2 perinuclear region with a contiguous array of 6×6

indentations at a rate of 10 μm/s and 30-nm (or 1.5-nN) relative indentation trigger. At least three different dishes were probed at a randomized order for each experiment. Force-depth curves were analyzed using non-Hertzian depth-dependent pointwise modulus as well as Hertzian-fitted apparent elastic modulus.[32]

Calcium Dynamics
Intracellular cytosolic Ca^{2+} dynamics was determined using the Fluo-4 AM calcium indicator (catalog #F14201; Thermo Fisher) according to the manufacturer's instructions. In brief, podocytes were plated on 25-mm round #1.5 coverslips (catalog #72290–12; EMS) at a density of 10,000 cells per slide, and they were differentiated for 9 days. They were then washed and switched overnight to serum-free RPMI medium for 24 hours before imaging. Cells were then loaded with Fluo-4 for 30 minutes at 37°C, washed, and switched to phenol-red–free imaging buffer (catalog #A14291DJ; Thermo Fisher). They were then transferred to stainless steel imaging chambers (catalog #A7816; Thermo Fisher) with 850 μl of imaging buffer and imaged on a Zeiss LSM 880 laser scanning confocal microscope using a 0.8 NA 20× air objective at 37°C with a frame rate of 1.5 seconds and uncropped scan resolution of 512×512 over a period of 25 minutes. Cells were stimulated for 5 minutes with 150 μl of FBS after acquisition of baseline conditions.

Podocyte Basal Motility Assay
Podocytes were plated on a 12-well plate at a density of 1000 cells per cm^2 and differentiated for 10–14 days at 37°C. Live-cell imaging was performed with a Leica DMi8 widefield microscope with a Pecon black-box environmental enclosure using a 0.32 NA 10× Leica phase contrast air objective with a rate of 32 frames per day over a period of 24 hours. Centroids of cells were tracked using a custom FIJI script in a semiautonomous manner by a blinded observer.

Podocyte Adhesion Dynamics Assay
Conditionally immortalized human podocytes expressing pan-nebulette shRNA or scrambled shRNA were each differentiated for 7 days at 37°C in RPMI media (catalog #11875119; Gibco) containing 2% FBS (catalog #26140079; Gibco) and 1% penicillin-streptomycin (catalog #15140122; Gibco) on six-well plates (140675; Nunc). One well of each cell type was washed with PBS before the addition of serum-free RPMI media with CellTracker Red CMTPX Dye (catalog #C34552; Invitrogen) or CellTracker Deep Red Dye (catalog #C34565; Invitrogen), to respective concentrations of 3.5 and 5 μM, for 45 minutes. After dye uptake, both wells were washed with PBS, and cells were trypsinized with 0.05% trypsin-EDTA (catalog #25300–054; Gibco). After trypsin neutralization, cells were transferred to separate 15-ml tubes, centrifuged at 1200 rpm for 5 minutes, and resuspended with RPMI. Media from each suspension were then combined at a 1:1 ratio of shRNA to scrambled cells. The well mixed

suspension of the two cell types was then seeded onto a six-well plate that had been coated with fibronectin (catalog #33016015; Gibco) at 10 μg/ml overnight. The plate was then immediately transferred onto a Leica DMi8 widefield microscope equipped with an enclosed humidity-controlled live-cell imaging chamber maintained at 37°C and 5% CO_2. To minimize the time between cell plating and imaging, the microscope settings had been set prior and brought to focus with an empty six-well plate. Regions of interest were marked, and the imaging was initiated within 15 minutes of plating. Fluorescent and brightfield images were taken every 5 minutes with a 20× 0.5 NA objective using Leica LAS X software (version 3.7.0.20979). To minimize the effect of stage movement on cell spreading, stage speed was lowered not to exceed 3 mm/s and acceleration was lowered not to exceed 398 μm/s^2.

Western Blot Analysis

Cellular proteins were extracted using a lysis buffer containing protease and phosphatase inhibitor cocktail (catalog #78440; Thermo Scientific). Equal amounts of protein lysates were separated by gel electrophoresis and transferred to 0.45-μm nitrocellulose membranes (catalog #1620145; Bio-Rad Laboratories). The membranes were probed with the following antibodies: rabbit anti–actinin-4 (catalog #ab108198; Abcam), mouse anti-myc tag (catalog #ab32; Abcam), rabbit anti-nebulette (Isoform-1, catalog #NBP1–86463; Novus), goat anti–LIM-nebulette (Isoform-2, catalog #NBP1–45223; Novus) mouse anti-vimentin (catalog #ma5–11883; Invitrogen), and mouse anti-tubulin (catalog #T6199; Sigma-Aldrich). We note that isoform-1–specific rabbit anti-nebulette antibody was used only to confirm the downstream phenotype of the KO animals (i.e., complete KO in the heart) and the specificity of isoform-2 in the kidney glomerulus.

Immunoprecipitation

Cells were collected and lysed with immunoprecipitation (IP) lysis buffer (25 mM Tris, 150 mM NaCl, 1 mM EDTA, 1% Triton-X) containing inhibitor cocktails. Protein complexes were immunoprecipitated using DynaBeads M-280 Sheep anti-Mouse IgG (catalog #11202D; Life Technologies) for 6 hours with (or without) monoclonal [9E10] myc-tag mouse monoclonal antibodies (catalog #ab32; Abcam) and washed with the wash buffer (1 M NaCl+0.1% Tween-20). The beads were pulled down using the DynaBeads magnet system, according to manufacturer's protocol. Precipitates for anti–myc-tag, negative control (beads incubated with mouse IgG), and total lysates were analyzed using gel electrophoresis followed by western blotting, and the results were quantified as previously described.[33]

Statistical Analyses

Analyses and visualization of data were performed with Matlab 2018A (Mathworks) or Prism 6.0 (GraphPad Software). All HCA data are reported as median±interquartile range, whereas low-content data are reported as mean±SD unless otherwise noted. For comparison of human glomerular protein expression and animal timecourse data, ANOVA with *post hoc* Tukey test was used to evaluate statistical difference between groups. A *P* value <0.05 was considered statistically significant. For all HCA data, the Kruskal–Wallis unpaired nonparametric *t* test was used to compare experimental and control groups, and a *P* value of 0.01 or less was considered significant. For *in situ* PCR, quantitative histopathology, electron microscopy, AFM indentations, and GTPase activity G-LISA assays, where multiple measures from a single animal or cell were combined (*e.g.*, multiple glomeruli in histology), nonparametric mixed model of ANOVA was used to compare WT and KO groups, whereby samples were treated as a fixed effect and repeated measures were treated as a random effect. A *P* value <0.05 was considered statistically significant. All experiments were repeated independently at least twice with new biologic material.

RESULTS

LIM-Nebulette Is a Podocyte-Specific Protein Downregulated in PAN-Induced Nephrotic Rats

We identified LIM-nebulette through an unbiased proteomic screen using the PAN-induced nephropathy model in the rat. Adult male Sprague Dawley rats (*n*=6, each group) were injected with either PBS (vehicle) or a single dose of 100 mg/kg PAN through the tail vein and allowed to recover over a 4-week timecourse. Rats administered with a single dose of PAN developed significant proteinuria within 1 week (Figure 1A), accompanied with significant renal hypertrophy (Figure 1B); however, evidence of glomerular injury, including foot process effacement, fully recovered within a month with no signs of prior damage (Figure 1C). Our hypothesis was that the expression of proteins that are key for the maintenance of podocyte morphology and foot process integrity would have a similar temporal change to that of filtration barrier integrity. To test this hypothesis, rats were euthanized at 1, 3, 7, 14, 21, and 28 days postinjection, and glomeruli were prepared for proteomics through sieving and flash-freezing in liquid nitrogen as previously described.[20] Differential glomerular protein expression was quantified as a function of time using isobaric labeled proteomics (Figure 1D). The topmost downregulated proteins in PAN-treated glomeruli included many podocyte-specific cytoskeletal and slit diaphragm proteins that are critical for podocyte-associated biologic processes (Supplemental Figure 1), in agreement with our original hypothesis.

When ranked by severity of loss of protein expression, the most consistently downregulated protein in PAN-treated glomeruli was nebulette (Supplemental Figure 2). This temporal pattern of reduced protein expression was also observed at the RNA level, where *Nebl* expression was significantly downregulated similar to slit diaphragm components nephrin and podocin (Figure 1E). Mostly known for its role in stabilization of cardiac sarcomeres,[34] nebulette translates into an
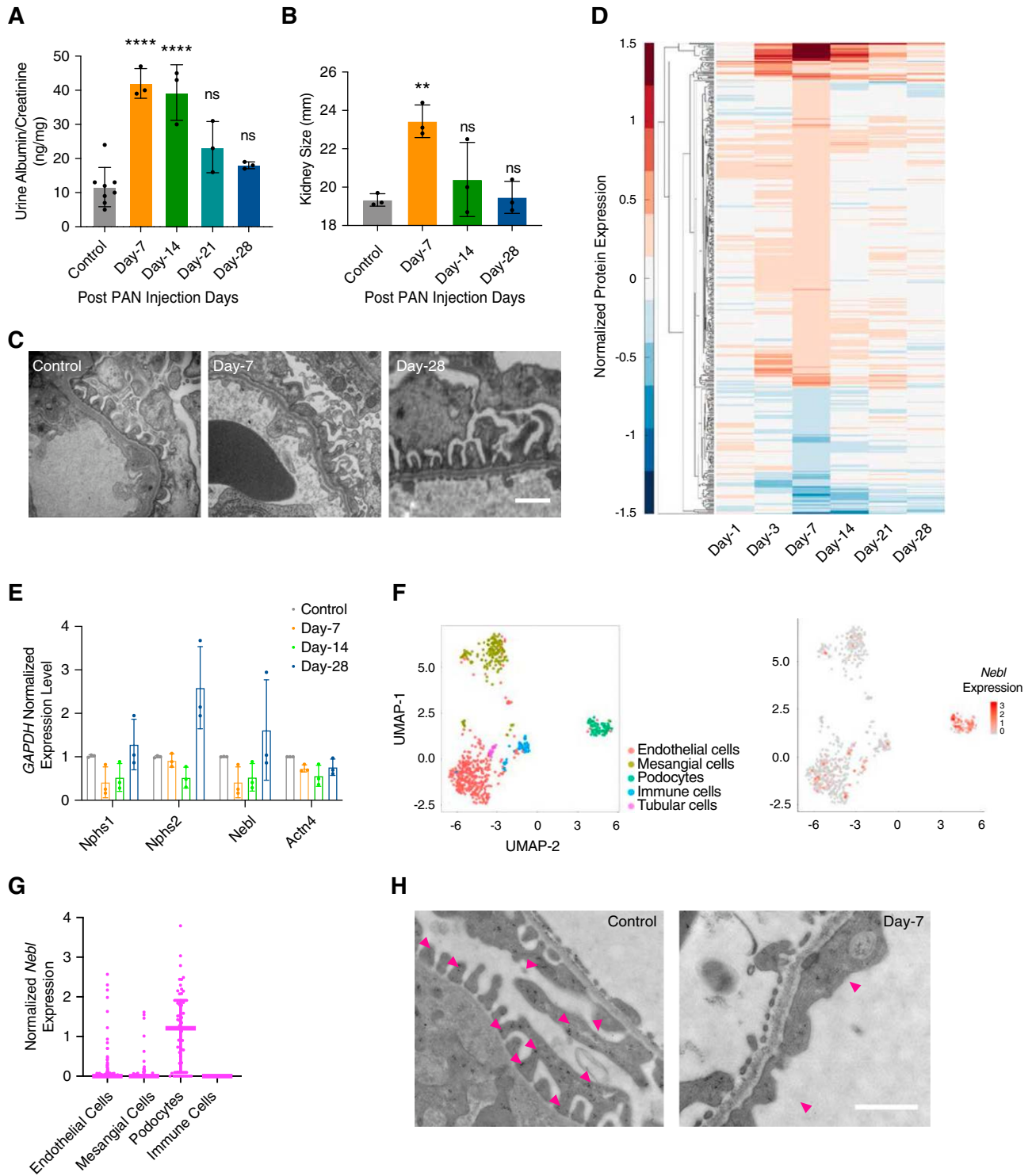
Figure 1. Transient PAN nephropathy model in the rat shows that LIM-nebulette expression correlates with glomerular function. (A) Adult Sprague Dawley rats injected with 100 mg/kg PAN develop transient proteinuria as measured by albumin–creatinine ratio (****$P<0.001$; one-way ANOVA with *post hoc* Tukey, $n=8$ in control, $n=3$ at postinjection time points). (B) Kidneys exhibit significant yet transient hypertrophy (**$P<0.01$; one-way ANOVA with *post hoc* Tukey, $n=3$ at each time point). (C) Podocytes develop diffuse foot process effacement that is resolved in 28 days (scale bar, 2 μm). (D) Isobaric-labeled shotgun proteomics using the iTRAQ method consistently identifies 512 proteins enriched in the glomeruli, of which LIM-nebulette is the protein with the highest reduction in expression level at day 7 postinjection. (E) Transient loss of *Nebl* expression is recapitulated at the RNA level as measured by quantitative RT-PCR, and it mimics podocyte marker *Actn4* and slit diaphragm proteins *Nphs1* and *Nphs2* ($n=3$ at each time point). (F)

actin-associated protein that has two known major iso-forms, which share C termini, but have distinct promoter sites within the *NEBL* gene.[35] The first (and canonical) iso-form, which is commonly referred to as nebulette, is thought to be cardiac-specific, and it was shown to be asso-ciated with dilated cardiomyopathy as a mechanosensitive component within the cardiac sarcomere.[36] Isoform-2, more commonly known as Lasp-2 or LIM-nebulette (here-after referred to as LIM-nebulette), was originally discov-ered in the brain, and it was shown to localize in focal adhesions and to play a role in cell migration.[37] LIM-nebulette is a smaller cleaved form that includes a unique LIM domain (hence the name), and it shares the carboxyl-terminal Src homology-3 (SH3) domain but lacks most of the nebulin repeat domains.[38] The quantity of identified peptides within our proteomic screen revealed no peptides unique to the larger nebulette isoform-1 except for those common to the C terminus (Supplemental Figure 3), sug-gesting that the isoform we have observed is indeed LIM-nebulette. Because the two isoforms lead to two distinct proteins, we carefully picked antibodies that can selectively recognize epitopes unique to either of the proteins to vali-date their expression (Supplemental Figure 4). Accordingly, throughout the study, unless differentially specified, all as-says were carried out using antibodies specifically raised against LIM-nebulette (or isoform-2) only.

Despite the prominent podocyte signature, our proteomic screen used glomeruli, not isolated podocytes. In order to de-finitively determine which cell type(s) expressed *Nebl*, we per-formed single-cell RNA sequencing (scRNAseq) in isolated glomeruli of WT mice, where we can identify podocytes as well as immune, mesangial, and endothelial cells as previously reported[23] (Figure 1F, left panel). The *Nebl* transcript was al-most exclusively detected in podocytes (Figure 1F, right panel), which formed the only cluster with a median expres-sion level that was significantly different from zero (Figure 1G). Similarly, reanalysis of publicly available single-nuclear RNA sequencing data[39,40] for human cortical isolates showed that *NEBL* expression in the human kidney is also strongly confined to podocytes (Supplemental Figure 5). STED and Airyscan super-resolution images of healthy ne-phrectomy samples from human kidneys, stained with anti–LIM-nebulette and anti–actinin-4 antibodies, showed that LIM-nebulette expression was detected in visceral epithe-lial cells positive for actinin-4 (Supplemental Figure 6). Im-munogold labeling in the rat also showed that LIM-nebulette expression is mostly detected in primary, secondary, and ter-tiary (foot) processes of podocytes, and further confirmed that

its expression is reduced during PAN-induced nephropathy (Figure 1H).

Nebulette KO Mice Are More Sensitive to Glomerular Injury

To determine the functional role of LIM-nebulette *in vivo*, we used a previously established $Nebl^{-/-}$ mouse line (Strain 07146; EMMA) that was backcrossed into C57BL/6J back-ground (Strain 000664; The Jackson Laboratory). These animals were shown to have a full KO for nebulette and a significantly reduced expression for LIM-nebulette. They were further shown to have a mild sarcomeric architecture phenotype during cardiac injury, but otherwise had normal life expectancy.[41] We confirmed by western blotting that in the $Nebl^{-/-}$ mice nebulette isoform-1 was knocked out in the heart, and that LIM-nebulette expression was significantly di-minished in the glomeruli (Figure 2A). Immunofluorescence staining for LIM-nebulette in the kidneys showed significantly reduced glomerular expression (Figure 2B). Because there was no overt renal phenotype at baseline (Supplemental Figure 7), we challenged these animals with 15 mg/kg ADR *via* retroor-bital injection. As expected, given their background strain resistance to glomerular disease, the phenotype for the WT animals was mild. However, $Nebl^{-/-}$ KO animals lost more weight after ADR injection (Figure 2C) and developed signif-icant proteinuria within 2 weeks that was sustained over the course of 28 days (Figure 2D, Supplemental Figure 8). Quan-titative histopathologic analyses showed significant glomeru-lar hypertrophy accompanied by a significant reduction in WT-1–positive cells (Figure 2, E and F). Quantitative TEM imaging revealed widespread foot process effacement only in the ADR-injected KO animals (Figure 2, G and H; WT-PBS=389±57 nm, KO-PBS=392±59 nm, WT-ADR=397±60 nm, KO-ADR=468±93 nm; ****$P<0.001$). Taken together, these data suggest that LIM-nebulette plays a functional role in maintenance of podocyte foot process architecture.

LIM-Nebulette Plays a Role in Cell Adhesion, Migration, Calcium Handling, and Rho GTPase Activity in Primary Mouse Podocytes

In order to understand the physiologic role of LIM-nebulette in podocyte function, we isolated primary podocytes from age- and sex-matched WT and KO littermates as previously described.[24] Before each phenotypic assay, cells were con-firmed to be positive for nuclear WT-1 expression (Supplemental Figure 9). Isolated KO primary podocytes were significantly smaller with smaller nuclei compared with

---

Uniform Manifold Approximation and Projection (UMAP) plot shows that scRNAseq of isolated glomerular cells using the Fluidigm C1 system identifies all major cellular components in the glomerulus, (G) and that *Nebl* expression is almost exclusively detected in the podocytes. (H) Immunogold labeling in the rat shows that expression of LIM-nebulette is mostly confined to processes of kidney podocytes (in particular to the cytoplasmic sites near the slit diaphragm), and it is substantially reduced in the effaced foot processes during PAN nephropathy (scale bar, 2 μm).
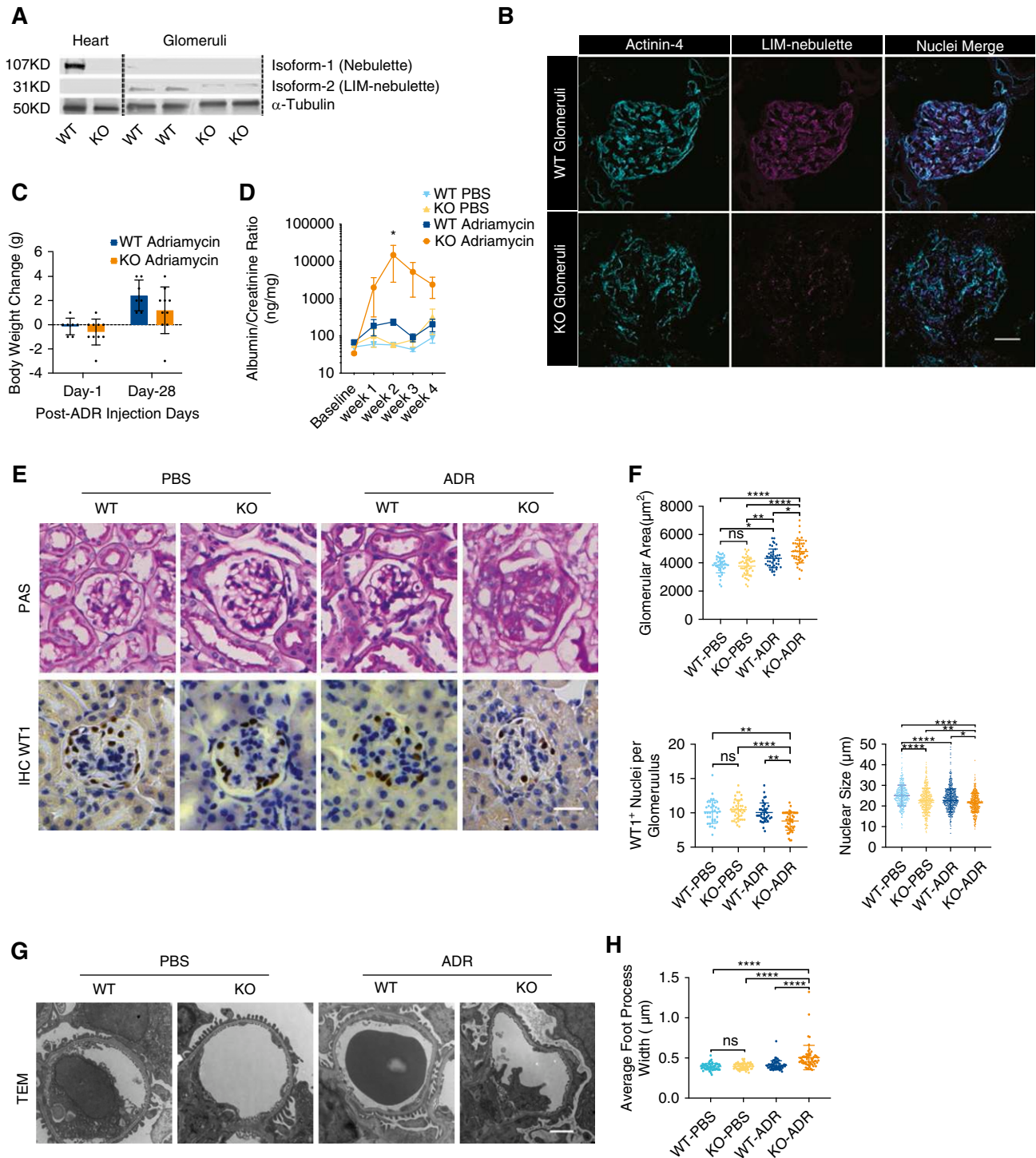
Figure 2. $Nebl^{-/-}$ KO mice are more sensitive to glomerular injury. (A) KO of isoform-1 (nebulette) in the hearts and isoform-2 (LIM-nebulette) in the glomeruli of transgenic mice backcrossed into resistant C57BL/6J background was confirmed using western blotting and (B) immunofluorescence staining (scale bar, 50 μm). (C) KO mice displayed higher weight loss compared with WT animals upon ADR injection ($n=7–10$ mice in each group). (D) They further developed significant and persistent proteinuria at 4 weeks compared with the mild proteinuria observed in the WT resistant background (*$P<0.05$; two-way ANOVA, $n=7–10$ mice in each group). (E) In tissues collected at 4 weeks, periodic acid–Schiff (PAS) staining further shows substantial sclerosis and glomerular hypertrophy in KO-ADR animals only (scale bar, 50 μm). (F) Quantitative morphometric analysis shows increased glomerular hypertrophy and decreased number of WT-1–positive nuclei only in KO-ADR animals but not in WT-ADR or PBS-injected animals (*$P<0.05$, **$P<0.01$, ****$P<0.001$; repeated measures ANOVA with *post hoc* Tukey, $n=5$ mice with 104–172 glomeruli for each group). (G) TEM shows

WT (Figure 3A). We used our previously established automated quantitative morphometric assay[6] to monitor over a dozen image-based cellular and subcellular parameters related to cytoplasmic, nuclear, cytoskeletal, and focal adhesion-related morphologic attributes. In addition to their smaller spreading area, we noted that KO podocytes displayed thinner and shorter actinin-4–crosslinked actin stress fibers, fewer peripheral projections, fewer and shorter focal islands per adhesive area, and lower colocalization of actinin-4 with paxillin (Figure 3B; **$P<0.01$, ***$P<0.001$, ****$P<0.001$).

Because *NEBL* mutations in patients were previously associated with calcium handling defects in cardiomyocytes,[34] we investigated calcium handling dynamics in KO podocytes. When primary podocytes were serum-starved overnight and then stimulated with FBS, they showed a robust transient uptake of calcium (Figure 3C, Supplemental Video 1). The peak amplitude and the first derivative of activation of calcium uptake were both significantly higher in KO cells compared with WT cells (Figure 3D; *$P<0.05$).

Aberrant focal adhesion morphometrics and calcium handling suggested that LIM-nebulette might play a role in adhesion and migration dynamics of podocytes. We therefore tracked the undirected motility of cultured WT and KO primary podocytes under basal conditions. On average, KO cells traversed significantly smaller distances over the course of 24 hours, with a significantly lower instantaneous velocity (Figure 3E; *$P<0.05$, ***$P<0.001$). Because the changes in focal adhesion and cytoskeletal dynamics are highly interrelated to Rho GTPases, we then checked the activity level of RhoA in freshly isolated glomeruli from WT and KO animals. Overall, glomeruli from KO animals exhibited significantly lower RhoA levels compared with those from WT animals (Figure 3F; **$P<0.01$).

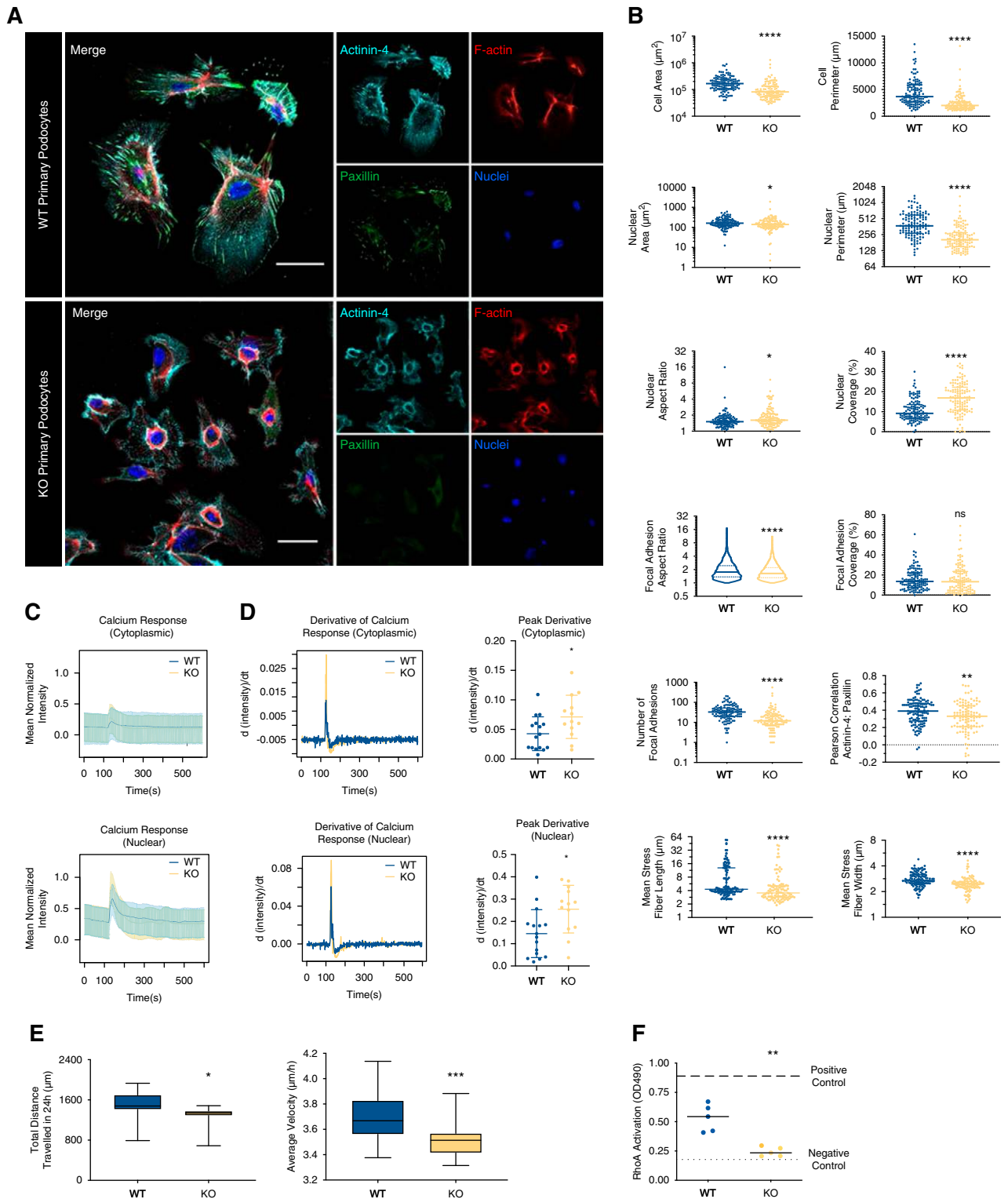## LIM-Nebulette Expression Is Significantly Reduced in Human Disease at Both Transcript and Protein Level

Next, we evaluated the level of expression of LIM-nebulette in human kidneys during health and disease, first by using the NephroSeq database,[42] which showed significant downregulation of *NEBL* at the transcript level in both the DN and FSGS datasets (Figure 4A; **$P<0.01$, ****$P<0.001$). Because the NephroSeq database is limited to transcriptomic data, we used internal formalin-fixed, paraffin-embedded cortical tissue samples ($n=7$) to evaluate the amount and distribution of LIM-nebulette protein expression in both healthy and diseased kidney tissues. Immunofluorescence imaging after antigen retrieval showed that the distribution of LIM-nebulette in the human kidneys mirrored those in

the rat and mouse, with localization in the visceral epithelial cells in agreement with the scRNAseq results (Figure 4B). Similar to the NephroSeq results, there was a significant reduction in LIM-nebulette protein expression in patients with FSGS and in patients with DN (Figure 4C; ***$P<0.001$, ****$P<0.001$).

LIM-Nebulette Colocalizes with Focal Adhesions as Well as Intermediate Filaments in Human Podocytes *In Vitro* and *In Vivo*

We next assessed the level of LIM-nebulette expression in human podocytes using an established immortalized human podocyte cell line[43] as well as an hiPSC-derived podocyte line that was developed following a recently established protocol.[44] In the immortalized podocyte cell line, the level of LIM-nebulette expression increased after 10 days of differentiation by thermoshifting to 37°C (Supplemental Figure 10A). Immunofluorescence staining showed that LIM-nebulette expression in the differentiated cells was mostly colocalized with actinin-4 and the actin cytoskeleton with slight nuclear expression in some cells (Supplemental Figure 10B). In hiPSC-derived podocytes, which have been shown to have higher levels of differentiation markers following the established directed differentiation protocol,[27] we saw a more robust expression of LIM-nebulette in the peripheral focal adhesions (which was in agreement with the increasingly robust actin cytoskeleton and the highly arborized morphology more similar to freshly isolated primary podocytes; Supplemental Figure 11). Interestingly, spatial expression of LIM-nebulette outside the actinin-4–positive focal adhesions in these cells was more filamentous and perinuclear (Figure 5A). Using triple immunostaining of LIM-nebulette, intermediate filament vimentin, and actinin-4 (along with F-actin stress fibers and nuclei), we showed that LIM-nebulette simultaneously localizes with the intermediate filaments in the cell body and with actinin-4–positive focal adhesions in the cell periphery. These results, in agreement with the distribution observed in human kidney section images obtained with super-resolution STED imaging (Supplemental Figure 6A), suggested that LIM-nebulette could be a rare podocyte-specific marker that may be spatially localized to both primary and tertiary (foot) processes. We tested this *in vivo* using triple immunostaining of LIM-nebulette, vimentin, and actinin-4 in frozen cortical tissues of healthy nephrectomy samples using super-resolution Airyscan laser scanning confocal microscopy. Our results showed that LIM-nebulette indeed colocalized with vimentin in the primary processes and with actinin-4 in the foot processes of podocytes (Figure 5B).

widespread foot process effacement only in the KO-ADR group (scale bar, 2 μm); (H) average foot process width was significantly different from all other groups (*$P<0.05$, ****$P<0.001$; repeated measures ANOVA with *post hoc* Tukey, $n=5$ mice with 59–61 glomeruli in each group).

Figure 3. LIM-nebulette plays key cell biologic roles in primary mouse podocytes. (A) Representative confocal immunofluorescence images of primary mouse podocytes isolated from WT or $Nebl^{-/-}$ mice (KO) stained for focal adhesion marker paxillin (green), actin crosslinker actinin-4 (cyan), F-actin (red), and nuclei (blue; scale bars, 50 μm). (B) HCA shows that KO cells ($n=121$) have significantly different focal adhesion, cellular, nuclear, and cytoskeletal morphometrics including smaller spreading area and nuclei, fewer and shorter focal adhesions, and thinner and shorter stress fibers (*$P<0.05$, **$P<0.01$, ****$P<0.001$; nonparametric unpaired t test, $n_{WT}=121$, $n_{KO}=120$). Live-cell imaging using Fluo-4 calcium sensor shows that both (C) the amplitude and (D) the rate of transient
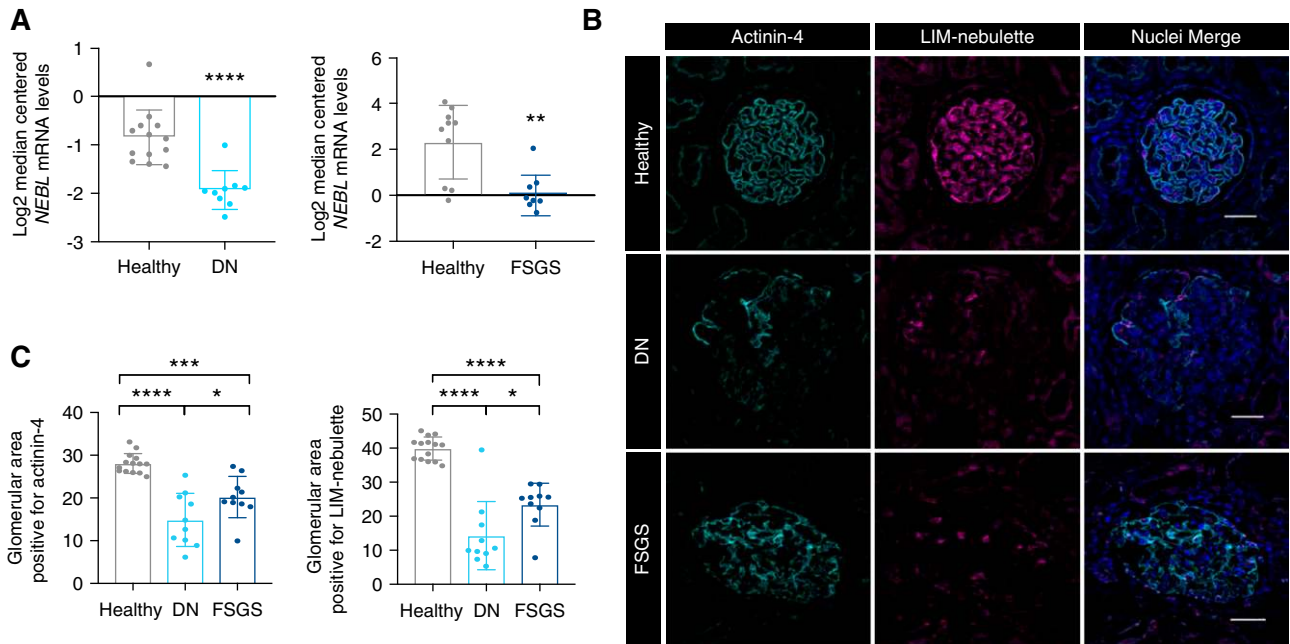
Figure 4. LIM-nebulette expression is significantly reduced in human disease at both transcript and protein level. (A) Mining of the NephroSeq database shows that mRNA expression levels of *NEBL* are significantly reduced in both DN and FSGS cases (**$P<0.01$, ****$P<0.001$; nonparametric unpaired *t* test, $n=8–13$ cases in each group). (B) Representative images that show the spatial protein expression of LIM-nebulette (and actinin-4 as positive control) from healthy nephrectomy versus DN and FSGS cases after formalin fixation, paraffin embedding, and immunofluorescent staining using antigen retrieval (scale bars, 50 μm). (C) Protein expression levels as estimated by the percentage of glomerular area positively stained after segmentation and grayscale thresholding (*$P<0.05$, ***$P<0.001$, ****$P<0.001$; one-way ANOVA with *post hoc* Tukey test, $n=4$ cases with 20–34 glomeruli in each group).

LIM-Nebulette Knockdown Leads to Dysregulation of Intermediate Filament Architecture and Compromises Cell Biomechanics

In order to assess the potential functional role of LIM-nebulette in the dynamics of actin and intermediate filament cytoskeleton, we created a stable LIM-nebulette knockdown human podocyte cell line *via* transduction with a lentivector expressing a p an-nebulette shRNA (Supplemental Figure 12). Human pan-nebulette shRNA-expressing cells displayed smaller spreading area with shorter actin stress fibers similar to what was observed in primary mouse podocytes. In agreement with the primary cell measurements, LIM-nebulette silencing also led to aberrant adhesive properties, where LIM-nebulette knockdown cells were spreading at 3.127 μm^2/s compared with 25.953 μm^2/s in scrambled cells (Figure 6A). In addition, LIM-nebulette silencing in human podocytes induced acute dysregulation of intermediate filaments (Figure 6B), with significantly decreased vimentin

distribution within the overall cell area and significantly altered filamentous textural properties as characterized by quantitative HCA (Figure 6C). To determine potential direct interaction of LIM-nebulette with vimentin, we stably overexpressed myc-tagged human LIM-nebulette protein in the immortalized human podocyte cell line, differentiated the cells at 37°C for 10–14 days, and performed myc-tag IP followed by western blotting. Both vimentin and actinin-4 were immunoprecipitated with myc-tagged LIM-nebulette (Figure 6D). Next, using arrays of AFM indentations to probe the biomechanical stability of intermediate filaments during nebulette knockdown, we confirmed that LIM-nebulette knockdown cells indeed exhibited significantly reduced elastic modulus in agreement with abnormal filamentous vimentin dynamics measured through HCA (Figure 6E). This reduced elastic modulus phenotype was also recapitulated in primary mouse podocytes isolated from WT and KO mice (Supplemental Figure 13). To test the bidirectional dynamics of this potential direct interaction, we

uptake of calcium (derivative of intensity) are significantly affected in KO cells (*$P<0.05$; nonparametric unpaired *t* test, $n=13–16$ cells for each independent experiment). Live-cell imaging also shows that basal cell motility is significantly altered in KO cells. (E) Total distance traversed in 24 hours, and average basal cellular velocity (*$P<0.05$, ***$P<0.001$; nonparametric unpaired *t* test, $n>900$ cells in each group). (F) Average RhoA GTPase activity levels, as measured by G-LISA, of freshly isolated and flash-frozen glomeruli from WT or KO mice show significant reduction in RhoA activity in KO podocytes (**$P<0.01$; repeated measures ANOVA, $n=6$).
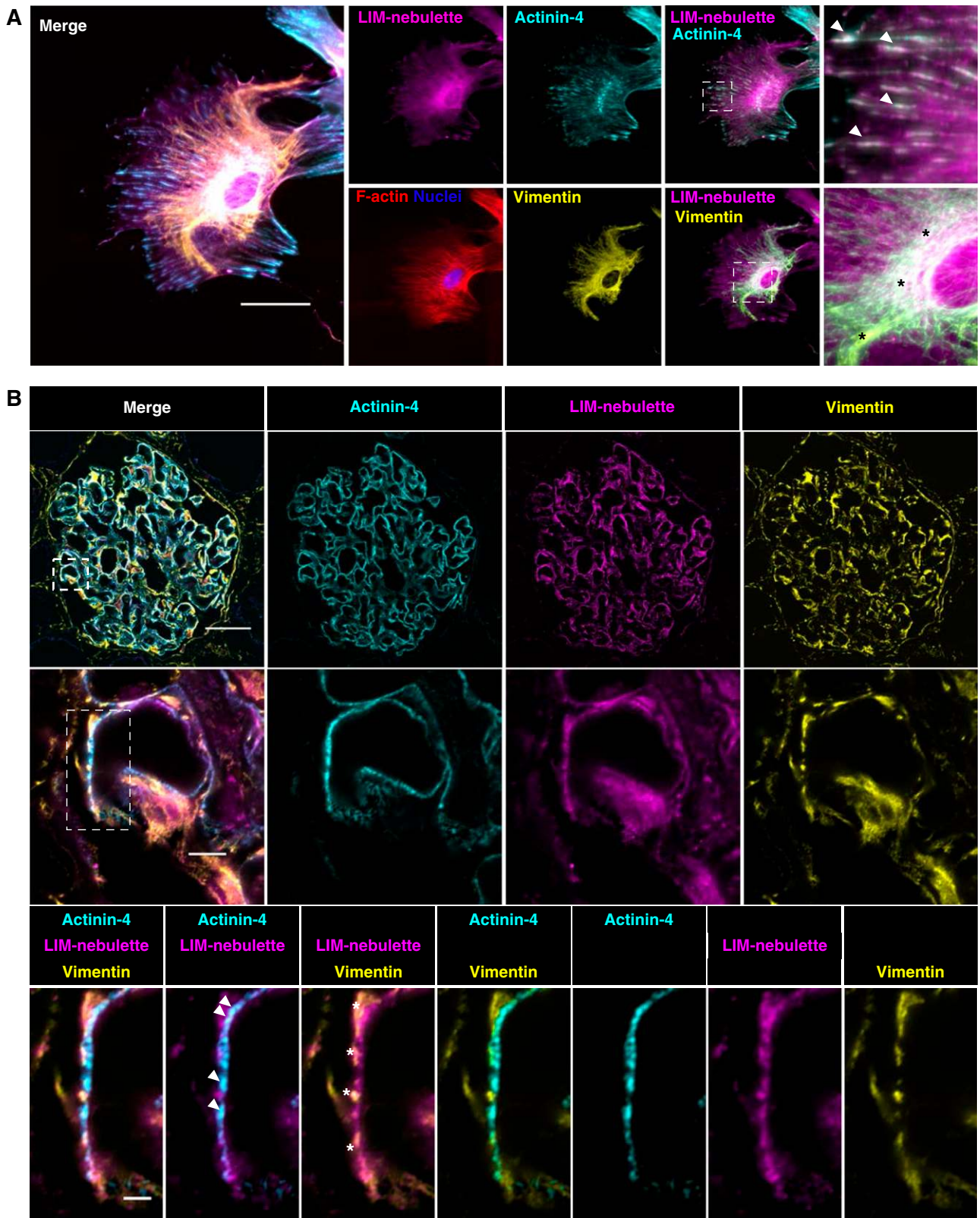
Figure 5. LIM-nebulette colocalizes with focal adhesions as well as intermediate filaments in human podocytes *in vitro* and *in vivo*. (A) Representative five-color immunofluorescence images showing that substantial LIM-nebulette (magenta) expression was detected in hiPSC-derived podocytes observed as punctate in the cell periphery and filamentous clusters in the perinuclear core. Arrows point to peripheral expression of LIM-nebulette that colocalizes with actinin-4 (cyan), whereas asterisks point to perinuclear expression of

evaluated the spatial distribution of nebulette in WT human podocyte cell lines that were treated with various cytoskeletal inhibitors (Supplemental Figure 14). Accordingly, podocytes treated with intermediate filament vimentin inhibitor arylquin-1 for 1 hour showed substantial spatial redistribution of LIM-nebulette from perinuclear to peripheral focal adhesion sites (Figure 6F), suggesting that shuttling of LIM-nebulette between the intermediate filament and actin-binding pools is a dynamic process. Taken together, these findings suggest that LIM-nebulette could be part of a complex with these proteins, and that it may play a role in the biomechanical stability of intermediate filaments in addition to focal adhesion remodeling.

DISCUSSION

In this study, we have established that LIM-nebulette, the second isoform of the *NEBL* gene product (also known as Lasp-2), is a podocyte-specific structural protein that plays a panoply of roles in podocyte physiology and biomechanics. In particular, its role as a potential intermediary between vimentin and actin filaments is unique. Although a number of similar actin-associated proteins have been shown to play a role in structural stability of the podocyte cytoskeleton and foot process architecture,[45,46] to the best of our knowledge, no protein in the podocyte has been shown to directly interact with intermediate filaments as well as actin fibers. This flexible portfolio is potentially very important in LIM-nebulette's functional role. Our acute cytoskeletal inhibition experiments using an array of actin stress fiber or vimentin filament disruptors (cytochalasin D, latrunculin B, withaferin A, or arylquin-1) consistently show that spatial distribution of LIM-nebulette is intricately tied to cytoskeletal stability. Dynamics of intermediate filaments are often overlooked in podocytes,[17] even though they are known to play a key role in cellular elasticity within the glomerulus,[14] and renal hyperfiltration of vimentin KO animals is known to show high levels of immediate mortality.[47] It should be noted that both isoforms of nebulette have been identified in the sarcomeric Z-discs, where a large cytoskeletal complex including intermediate filaments and actin crosslinkers is known to contribute to the remarkable stability[48] and spacing[49] of the cardiac sarcomere. One of the key unanswered questions in nephrology is the mechanism through which the podocyte maintains the strict spatial segregation of its cytoskeletal components in primary, secondary, and tertiary (foot) processes. It is possible that through its multidimensional role in cytoskeletal dynamics, LIM-nebulette could be one of the key players that maintain

this hierarchic order. Accordingly, we have schematically summarized the physiologic role of LIM-nebulette in podocytes, as measured within *in vivo* and *in vitro* contexts, in Figure 7.

The isoform specificity of nebulette is important and complicated. During the peer-review of this manuscript, a comprehensive study was published, investigating the role of the protein Lasp-1 in linking the slit diaphragm with the actin cytoskeleton in podocytes.[50] Lasp-1 is a key paralog of LIM-nebulette (also known as Lasp-2), which is the podocyte-specific isoform studied herein. It should be noted that although the second isoform of nebulette is also called Lasp-2, it is completely unrelated to the protein Lasp-1, which is encoded by the gene *LASP1*. Both the canonical first isoform and the second isoform of nebulette (*i.e.*, LIM-nebulette) are encoded by the same gene: *NEBL*. It is noteworthy that using RT-PCR, we saw no change in Lasp-1 levels in the glomeruli of our mice, and accordingly we ensured that our antibody epitopes had no overlap with Lasp-1.

Although its role in regulating the organization of multiple cytoskeletal species may be the most unusual characteristic of LIM-nebulette, it is important to note that this was one of the numerous facets of cell biologic alterations we had measured. LIM-nebulette's most studied role in focal adhesion organization and dynamics is particularly relevant for podocyte physiology and function. We have used automated HCA to thoroughly and quantitatively characterize the potential cell biologic roles of LIM-nebulette in an unbiased manner. One of the functional assays we had performed was an undirected cell motility assay, which showed that $Nebl^{-/-}$ primary mouse podocytes display decreased motility at baseline. As a binding partner for a number of adhesive and cytoskeletal proteins,[51,52] LIM-nebulette was shown to play both excitatory and inhibitory roles in focal adhesion turnover and motility in the context of different cancer cells.[52,53] Although podocytes *in situ* are thought to be relatively dormant in terms of lateral motility[54] and acquire an increased motile phenotype during dedifferentiation, the exact molecular role of LIM-nebulette in focal adhesion dynamics for adult podocytes *in vivo* could be different, and it will certainly require further molecular dissection in future studies. We also note that both calcium dynamics and Rho GTPase activity were significantly modified in KO animals. The changes in calcium activity in $Nebl^{-/-}$ cells could be due to LIM-nebulette's role as an adapter protein that brings calcium-dependent signaling proteins to the vicinity of key signaling hubs, such as focal adhesions or actin stress fibers. This in combination with altered focal adhesion architecture could result in aberrant Rho GTPase signaling, a key pathway in regulating podocyte structural integrity.

LIM-nebulette colocalizing with vimentin (yellow) intermediate filaments (scale bar, 50 μm). (B) This was recapitulated in human podocytes *in situ*; representative immunofluorescence images of healthy human glomerulus taken with Zeiss Airyscan super-resolution confocal microscope (top to bottom scale bars for each magnification are 50, 5, and 2 μm, respectively; arrows highlight LIM-nebulette colocalization with actinin-4, whereas asterisks point to LIM-nebulette colocalization with vimentin).
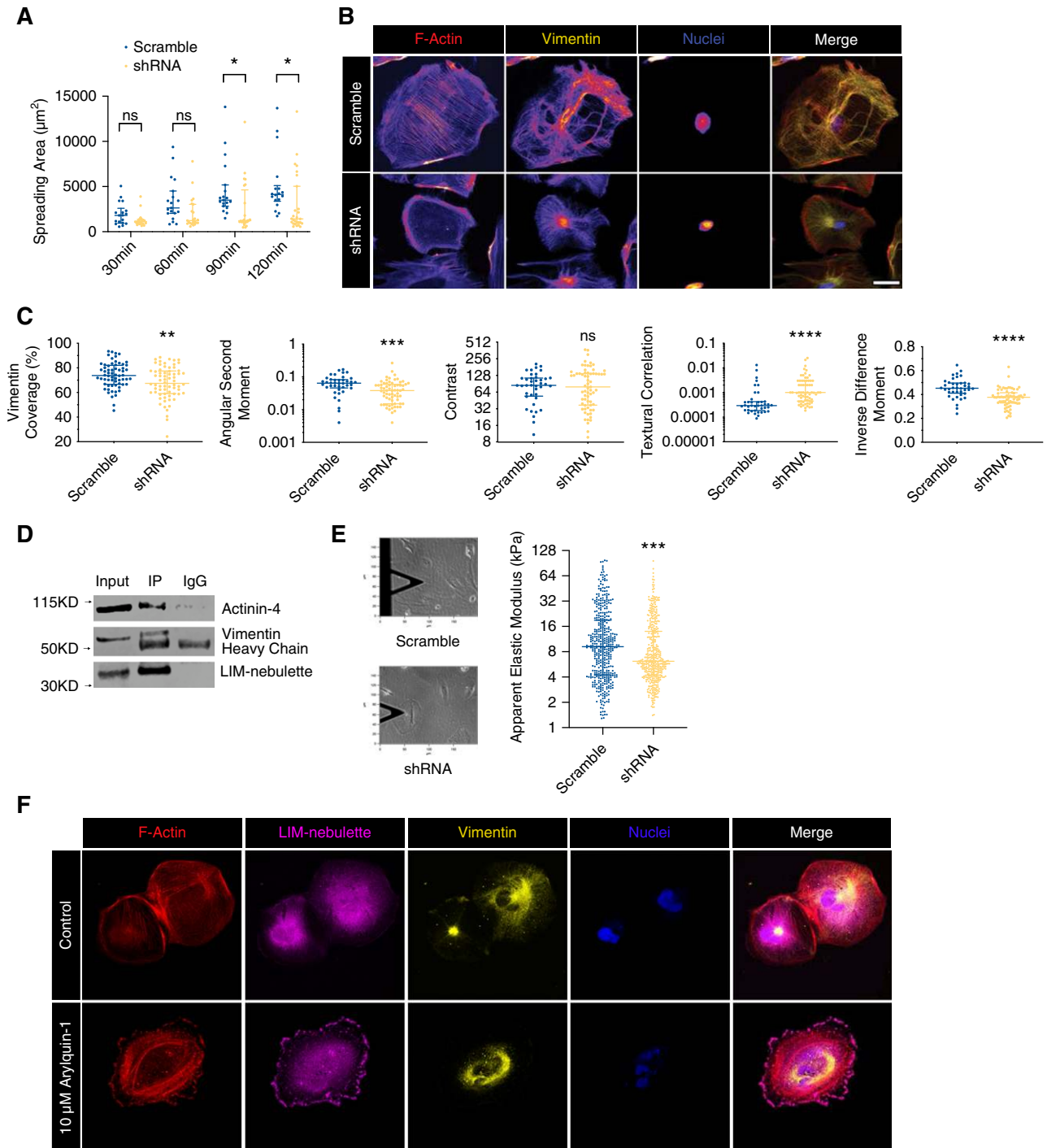
Figure 6. LIM-nebulette knockdown leads to dysregulation of intermediate filament architecture and compromises cell biomechanics. (A) Role of LIM-nebulette in cellular adhesion was evaluated by the rate of initial spreading of differentiated immortalized human podocytes stably expressing either scrambled or pan-nebulette shRNA. The rate of cell adhesion within 120 minutes postplating is significantly lower in LIM-nebulette–silenced podocytes (median rate of adhesion: 3.127 μm^2/s in shRNA versus 25.953 μm^2/s in scrambled; *$P<0.05$; two-way ANOVA with *post hoc* Tukey, $n=18$–27 cells in each group and time point). (B) Representative immunofluorescence images of scrambled or shRNA human podocytes showing differential cytoskeletal organization (scale bar, 50 μm). (C) Quantitative morphometrics using HCA show significant changes in area coverage of vimentin as well as several filamentous textural properties in LIM-nebulette shRNA cells (**$P<0.01$, ***$P<0.001$, ****$P<0.001$; nonparametric unpaired *t* test, $n=40$–70 cells in each group). (D) IP of ectopically expressed myc-tagged LIM-nebulette in immortalized human podocytes precipitates both vimentin and actinin-4. (E) Spatial arrays of AFM indentations show that the subcellular distribution of the apparent elastic modulus of
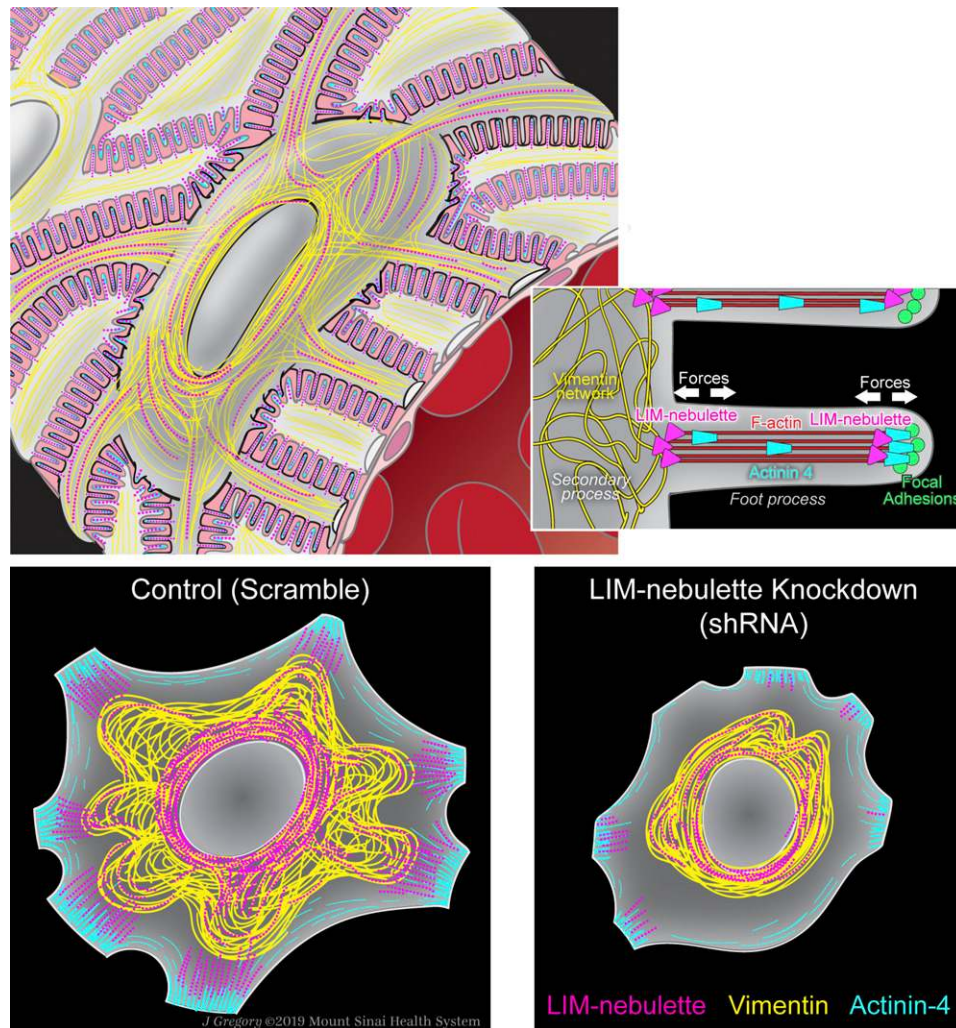
Figure 7. A working model of LIM-nebulette's cell biologic role in glomerular podocytes. LIM-nebulette is part of a stabilizing protein network bridging vimentin to crosslinked actin stress fibers, thereby increasing the biomechanical stability of podocyte processes. LIM-nebulette silencing causes acute dysregulation of podocyte intermediate filaments.

Nebulette was the most consistently downregulated protein in our proteomic assay of the PAN-nephropathy rats, which is coherent with the latter observations regarding the widespread spatial expression of LIM-nebulette in podocytes. Furthermore, we have consistently detected LIM-nebulette in almost all podocytes in our scRNAseq assays (as well as searches of publicly available scRNAseq data). Although it is clearly a highly abundant protein within the podocyte, the $Nebl^{-/-}$ animals had no apparent disease phenotype at baseline. This could be due to the incomplete KO of the second isoform of the gene or compensatory remodeling during development, which was a clear limitation of our animal model.

Alternatively, it is possible that LIM-nebulette's functional role may be more critical during stress conditions, due to its mechanosensitive role. It was previously shown that exogenously expressed GFP-tagged nebulette would rapidly translocate to the focal adhesions when the transfected muscle cells were mechanically stretched.[36] This stress-induced recruitment phenotype is consistent with the observations that $Nebl^{-/-}$ mice are healthy at baseline but are unable to respond to exogenous stress, hereby induced by ADR injection. In fact, despite being crossed into the resistant C57BL/6 background and being injected with only a single dose of ADR, $Nebl^{-/-}$ animals had a significant reduction in glomerular filtration

LIM-nebulette–silenced human podocytes differentiated for 10–14 days is significantly lower than control podocytes expressing scrambled shRNA (***$P<0.001$; repeated measures ANOVA with *post hoc* Tukey, $n=18$ cells in each group). (F) Immortalized WT human podocytes treated with 10 μM vimentin inhibitor arylquin-1 for 1 hour display a substantial alteration in spatial distribution of LIM-nebulette with increase peripheral expression (scale bar, 25 μm).

barrier integrity (including reduced podocyte number per glomerulus). Taken together with LIM-nebulette's strong physiologic and cell biologic roles in focal adhesion and calcium dynamics, this finding suggests that ADR-injured podocytes could likely have been detached due to adhesive abnormalities. In fact, our live-cell assay in immortalized human podocytes with shRNA knockdown of LIM-nebulette also showed impaired cell adhesion, further corroborating the key functional role of LIM-nebulette in podocyte adhesion dynamics.

It has been reported that communication between binding partners of different domains within LIM-nebulette is key for its subcellular localization.[55] There are numerous unique protein domains in LIM-nebulette that make it an interesting target as a multifunctional protein that may be essential for podocyte structural integrity and disease remodeling response. Aside from the SH3 domain that is strongly enriched in focal adhesions, perhaps the most interesting structural feature is its LIM domain. Proteins enriched for LIM domains have been shown to play key roles in focal adhesion maturation and stress fiber formation,[56] which are two of the key aspects of podocyte structural integrity.[57] In addition, the LIM domain has been shown to play a role in nuclear shuttling of proteins, thereby playing a role in transcriptional coregulation.[58] Although we have detected nuclear expression of LIM-nebulette in some differentiated immortalized human podocytes, the potential transcriptional regulatory role of LIM-nebulette requires further study, and it is beyond the scope of this investigation.

In this study, we have integrated isobaric-tagged proteomics, single-cell transcriptomics, super-resolution optical imaging, and AFM to show that LIM-nebulette is a new podocyte-specific protein that reinforces podocyte cytoskeletal integrity through its interactions with intermediate filaments, actin cytoskeleton, and focal adhesions. Even though our *in vitro* and *in vivo* assays have consistently shown the key role of LIM-nebulette, we think that we have only scratched the surface of LIM-nebulette's multifaceted role in podocyte physiology. Further investigation of its intracellular localization dynamics and additional cell biologic functions may give insights into morphologic specialization of the podocyte cytoskeleton. Moreover, elucidating different binding domains of LIM-nebulette and its binding partners may help to identify proteins that could be targeted to reinforce podocyte structural integrity and to slow down the progression of chronic glomerular diseases, such as FSGS and DN.

DISCLOSURES

All authors have nothing to disclose.

FUNDING

ACKNOWLEDGMENTS

DATA SHARING STATEMENT

All data supporting the findings of this manuscript are available from the corresponding author upon reasonable request. In addition, all of the raw and processed omics data are freely available in public databases. Raw counts and processed cell-based matrices for single-cell RNA sequencing data are available in the Gene Expression Omnibus with accession number GSE127235, whereas raw mass spectrometry data from iTRAQ proteomics are available in the ProteomeXchange Consortium via the PRIDE partner repository with the dataset identifiers PXD016629 and 10.6019/PXD016629. Processed and annotated results of the proteomics data are also included in Supplemental Table 2.

SUPPLEMENTAL MATERIAL

This article contains the following supplemental material online at http://jasn.asnjournals.org/lookup/suppl/doi:10.1681/ASN.2019121261/-/DCSupplemental.

Supplemental Table 1. Rat primers used for qRT-PCR.

Supplemental Table 2. Annotated proteomics results.

Supplemental Figure 1. Proteins downregulated in PAN-treated rat glomeruli.

Supplemental Figure 2. Nebulette protein expression and glomerular function.

Supplemental Figure 3. Proteomic screening of nebulette isoforms using mass spectrometry.

Supplemental Figure 4. Nebulette (isoform-1) and LIM-nebulette (isoform-2) epitopes.

Supplemental Figure 5. Analysis of glomerular/kidney *NEBL* expression in public databases.

Supplemental Figure 6. Super-resolution imaging of human glomeruli.

Supplemental Figure 7. Histopathologic assessment of *Nebl*$^{+/+}$ and *Nebl*$^{-/-}$ mice.

Supplemental Figure 8. Assessment of proteinuria in *Nebl*$^{+/+}$ and *Nebl*$^{-/-}$ mice.

Supplemental Figure 9. WT-1 expression in primary podocytes isolated from *Nebl*$^{+/+}$ and *Nebl*$^{-/-}$ mice.

Supplemental Figure 10. LIM-nebulette expression in immortalized human podocytes.

Supplemental Figure 11. Morphology of hiPSC podocytes.

Supplemental Figure 12. Protein expression in LIM-nebulette knockdown podocyte cell line.

Supplemental Figure 13. Cellular elasticity of primary mouse podocytes measured by AFM.

Supplemental Figure 14. LIM-nebulette spatial distribution in cells treated with cytoskeletal disruptors.

Supplemental Video 1. Calcium uptake by *Nebl*$^{-/-}$ podocytes.

REFERENCES

1. Endlich N, Endlich K: The challenge and response of podocytes to glomerular hypertension. *Semin Nephrol* 32: 327–341, 2012
2. Rinschen MM, Grahammer F, Hoppe AK, Kohli P, Hagmann H, Kretz O, et al: YAP-mediated mechanotransduction determines the podocyte's response to damage. *Sci Signal* 10: eaaf8165, 2017
3. Ziembicki J, Tandon R, Schelling JR, Sedor JR, Miller RT, Huang C: Mechanical force-activated phospholipase D is mediated by G$\alpha_{12/13}$-Rho and calmodulin-dependent kinase in renal epithelial cells. *Am J Physiol Renal Physiol* 289: F826–F834, 2005
4. Wyss HM, Henderson JM, Byfield FJ, Bruggeman LA, Ding Y, Huang C, et al: Biophysical properties of normal and diseased renal glomeruli. *Am J Physiol Cell Physiol* 300: C397–C405, 2011
5. Embry AE, Liu Z, Henderson JM, Byfield FJ, Liu L, Yoon J, et al: Similar biophysical abnormalities in glomeruli and podocytes from two distinct models. *J Am Soc Nephrol* 29: 1501–1512, 2018
6. Calizo RC, Bhattacharya S, van Hasselt JGC, Wei C, Wong JS, Wiener RJ, et al: Disruption of podocyte cytoskeletal biomechanics by dasatinib leads to nephrotoxicity. *Nat Commun* 10: 2061, 2019
7. Li K, Wang J, Yin X, Zhai X, Li Z: Alteration of podocyte protein expression and localization in the early stage of various hemodynamic conditions. *Int J Mol Sci* 14: 5998–6011, 2013
8. Hu M, Azeloglu EU, Ron A, Tran-Ba KH, Calizo RC, Tavassoly I, et al: A biomimetic gelatin-based platform elicits a pro-differentiation effect on podocytes through mechanotransduction. *Sci Rep* 7: 43934, 2017
9. Shankland SJ: The podocyte's response to injury: Role in proteinuria and glomerulosclerosis. *Kidney Int* 69: 2131–2147, 2006
10. Falkenberg CV, Azeloglu EU, Stothers M, Deerinck TJ, Chen Y, He JC, et al: Fragility of foot process morphology in kidney podocytes arises from chaotic spatial propagation of cytoskeletal instability. *PLOS Comput Biol* 13: e1005433, 2017
11. Faul C, Asanuma K, Yanagida-Asanuma E, Kim K, Mundel P: Actin up: Regulation of podocyte structure and function by components of the actin cytoskeleton. *Trends Cell Biol* 17: 428–437, 2007
12. Trickey WR, Vail TP, Guilak F: The role of the cytoskeleton in the viscoelastic properties of human articular chondrocytes. *J Orthop Res* 22: 131–139, 2004
13. Sistani L, Rodriguez PQ, Hultenby K, Uhlen M, Betsholtz C, Jalanko H, et al: Neuronal proteins are novel components of podocyte major processes and their expression in glomerular crescents supports their role in crescent formation. *Kidney Int* 83: 63–71, 2013
14. Embry AE, Mohammadi H, Niu X, Liu L, Moe B, Miller-Little WA, et al: Biochemical and cellular determinants of renal glomerular elasticity. *PLoS One* 11: e0167924, 2016
15. Boerries M, Grahammer F, Eiselein S, Buck M, Meyer C, Goedel M, et al: Molecular fingerprinting of the podocyte reveals novel gene and protein regulatory networks. *Kidney Int* 83: 1052–1064, 2013
16. Chen J, Boyle S, Zhao M, Su W, Takahashi K, Davis L, et al: Differential expression of the intermediate filament protein nestin during renal development and its localization in adult podocytes. *J Am Soc Nephrol* 17: 1283–1291, 2006
17. Schell C, Huber TB: The evolving complexity of the podocyte cytoskeleton. *J Am Soc Nephrol* 28: 3166–3174, 2017
18. Moncman CL, Wang K: Nebulette: A 107 kD nebulin-like protein in cardiac muscle. *Cell Motil Cytoskeleton* 32: 205–225, 1995
19. National Research Council (US) Committee for the Update of the Guide for the Care and Use of Laboratory Animals: *Guide for the Care and Use of Laboratory Animals*, Washington, DC, National Academies Press (US), 2011
20. Azeloglu EU, Hardy SV, Eungdamrong NJ, Chen Y, Jayaraman G, Chuang PY, et al: Interconnected network motifs control podocyte morphology and kidney function. *Sci Signal* 7: ra12, 2014
21. Jain MR, Li Q, Liu T, Rinaggio J, Ketkar A, Tournier V, et al: Proteomic identification of immunoproteasome accumulation in formalin-fixed rodent spinal cords with experimental autoimmune encephalomyelitis. *J Proteome Res* 11: 1791–1803, 2012
22. Jain MR, Liu T, Hu J, Darfler M, Fitzhugh V, Rinaggio J, et al: Quantitative proteomic analysis of formalin fixed paraffin embedded oral HPV lesions from HIV patients. *Open Proteomics J* 1: 40–45, 2008
23. Fu J, Akat KM, Sun Z, Zhang W, Schlondorff D, Liu Z, et al: Single-cell RNA profiling of glomerular cells shows dynamic changes in experimental diabetic kidney disease. *J Am Soc Nephrol* 30: 533–545, 2019
24. Zhong F, Chen H, Xie Y, Azeloglu EU, Wei C, Zhang W, et al: Protein S protects against podocyte injury in diabetic nephropathy. *J Am Soc Nephrol* 29: 1397–1410, 2018
25. Keenan AB, Jenkins SL, Jagodnik KM, Koplev S, He E, Torre D, et al: The library of integrated network-based cellular signatures NIH program: System-level cataloging of human cells response to perturbations. *Cell Syst* 6: 13–24, 2018
26. Carcamo-Orive I, Hoffman GE, Cundiff P, Beckmann ND, D'Souza SL, Knowles JW, et al: Analysis of transcriptional variability in a large human iPSC library reveals genetic and non-genetic determinants of heterogeneity. *Cell Stem Cell* 20: 518–532.e9, 2017
27. Musah S, Dimitrakakis N, Camacho DM, Church GM, Ingber DE: Directed differentiation of human induced pluripotent stem cells into mature kidney podocytes and establishment of a Glomerulus Chip. *Nat Protoc* 13: 1662–1685, 2018
28. Azeloglu EU, Albro MB, Thimmappa VA, Ateshian GA, Costa KD: Heterogeneous transmural proteoglycan distribution provides a mechanism for regulating residual stresses in the aorta. *Am J Physiol Heart Circ Physiol* 294: H1197–H1205, 2008
29. Tervaert TW, Mooyaart AL, Amann K, Cohen AH, Cook HT, Drachenberg CB, et al; Renal Pathology Society: Pathologic classification of diabetic nephropathy. *J Am Soc Nephrol* 21: 556–563, 2010

30. Chaudhry FA, Lehre KP, van Lookeren Campagne M, Ottersen OP, Danbolt NC, Storm-Mathisen J: Glutamate transporters in glial plasma membranes: Highly differentiated localizations revealed by quantitative ultrastructural immunocytochemistry. *Neuron* 15: 711–720, 1995

31. Azeloglu EU, Costa KD: Atomic force microscopy in mechanobiology: Measuring microelastic heterogeneity of living cells. *Methods Mol Biol* 736: 303–329, 2011

32. Azeloglu EU, Costa KD: Cross-bridge cycling gives rise to spatiotemporal heterogeneity of dynamic subcellular mechanics in cardiac myocytes probed with atomic force microscopy. *Am J Physiol Heart Circ Physiol* 298: H853–H860, 2010

33. Ron A, Azeloglu EU, Calizo RC, Hu M, Bhattacharya S, Chen Y, et al: Cell shape information is transduced through tension-independent mechanisms. *Nat Commun* 8: 2145, 2017

34. Maiellaro-Rafferty K, Wansapura JP, Mendsaikhan U, Osinska H, James JF, Taylor MD, et al: Altered regional cardiac wall mechanics are associated with differential cardiomyocyte calcium handling due to nebulette mutations in preclinical inherited dilated cardiomyopathy. *J Mol Cell Cardiol* 60: 151–160, 2013

35. Deng XA, Norris A, Panaviene Z, Moncman CL: Ectopic expression of LIM-nebulette (LASP2) reveals roles in cell migration and spreading. *Cell Motil Cytoskeleton* 65: 827–840, 2008

36. Purevjav E, Varela J, Morgado M, Kearney DL, Li H, Taylor MD, et al: Nebulette mutations are associated with dilated cardiomyopathy and endocardial fibroelastosis. *J Am Coll Cardiol* 56: 1493–1502, 2010

37. Terasaki AG, Suzuki H, Nishioka T, Matsuzawa E, Katsuki M, Nakagawa H, et al: A novel LIM and SH3 protein (lasp-2) highly expressing in chicken brain. *Biochem Biophys Res Commun* 313: 48–54, 2004

38. Eulitz S, Sauer F, Pelissier MC, Boisguerin P, Molt S, Schuld J, et al: Identification of Xin-repeat proteins as novel ligands of the SH3 domains of nebulin and nebulette and analysis of their interaction during myofibril formation and remodeling. *Mol Biol Cell* 24: 3215–3226, 2013

39. Wu H, Uchimura K, Donnelly EL, Kirita Y, Morris SA, Humphreys BD: Comparative analysis and refinement of human PSC-derived kidney organoid differentiation with single-cell transcriptomics. *Cell Stem Cell* 23: 869–881.e8, 2018

40. Wu H, Malone AF, Donnelly EL, Kirita Y, Uchimura K, Ramakrishnan SM, et al: Single-cell transcriptomics of a human kidney allograft biopsy specimen defines a diverse inflammatory response. *J Am Soc Nephrol* 29: 2069–2080, 2018

41. Mastrototaro G, Liang X, Li X, Carullo P, Piroddi N, Tesi C, et al: Nebulette knockout mice have normal cardiac function, but show Z-line widening and up-regulation of cardiac stress markers. *Cardiovasc Res* 107: 216–225, 2015

42. Martini S, Eichinger F, Nair V, Kretzler M: Defining human diabetic nephropathy on the molecular level: Integration of transcriptomic profiles with biological knowledge. *Rev Endocr Metab Disord* 9: 267–274, 2008

43. Saleem MA, O'Hare MJ, Reiser J, Coward RJ, Inward CD, Farren T, et al: A conditionally immortalized human podocyte cell line demonstrating nephrin and podocin expression. *J Am Soc Nephrol* 13: 630–638, 2002

44. Musah S, Mammoto A, Ferrante TC, Jeanty SSF, Hirano-Kobayashi M, Mammoto T, et al: Mature induced-pluripotent-stem-cell-derived human podocytes reconstitute kidney glomerular-capillary-wall function on a chip. *Nat Biomed Eng* 1: 69, 2017

45. Kliewe F, Scharf C, Rogge H, Darm K, Lindenmeyer MT, Amann K, et al: Studying the role of fascin-1 in mechanically stressed podocytes. *Sci Rep* 7: 9916, 2017

46. Artelt N, Ludwig TA, Rogge H, Kavvadas P, Siegerist F, Blumenthal A, et al: The role of palladin in podocytes. *J Am Soc Nephrol* 29: 1662–1678, 2018

47. Terzi F, Henrion D, Colucci-Guyon E, Federici P, Babinet C, Levy BI, et al: Reduction of renal mass is lethal in mice lacking vimentin. Role of endothelin-nitric oxide imbalance. *J Clin Invest* 100: 1520–1528, 1997

48. Arimura T, Nakamura T, Hiroi S, Satoh M, Takahashi M, Ohbuchi N, et al: Characterization of the human nebulette gene: A polymorphism in an actin-binding motif is associated with nonfamilial idiopathic dilated cardiomyopathy. *Hum Genet* 107: 440–451, 2000

49. Balogh J, Li Z, Paulin D, Arner A: Desmin filaments influence myofilament spacing and lateral compliance of slow skeletal muscle fibers. *Biophys J* 88: 1156–1165, 2005

50. Lepa C, Möller-Kerutt A, Stölting M, Picciotto C, Eddy ML, Butt E, et al: LIM and SH3 protein 1 (LASP-1): A novel link between the slit membrane and actin cytoskeleton dynamics in podocytes. *FASEB J* 34: 5453–5464, 2020

51. Li B, Zhuang L, Trueb B: Zyxin interacts with the SH3 domains of the cytoskeletal proteins LIM-nebulette and Lasp-1. *J Biol Chem* 279: 20401–20410, 2004

52. Bliss KT, Chu M, Jones-Weinert CM, Gregorio CC: Investigating lasp-2 in cell adhesion: New binding partners and roles in motility. *Mol Biol Cell* 24: 995–1006, 2013

53. Wang B, Zhang L, Zhao L, Zhou R, Ding Y, Li G, et al: LASP2 suppresses colorectal cancer progression through JNK/p38 MAPK pathway mediated epithelial-mesenchymal transition. *Cell Commun Signal* 15: 21, 2017

54. Endlich N, Siegerist F, Endlich K: Are podocytes motile? *Pflugers Arch* 469: 951–957, 2017

55. Nakagawa H, Suzuki H, Machida S, Suzuki J, Ohashi K, Jin M, et al: Contribution of the LIM domain and nebulin-repeats to the interaction of Lasp-2 with actin filaments and focal adhesions. *PLoS One* 4: e7530, 2009

56. Grunewald TG, Butt E: The LIM and SH3 domain protein family: Structural proteins or signal transducers or both? *Mol Cancer* 7: 31, 2008

57. Pozzi A, Jarad G, Moeckel GW, Coffa S, Zhang X, Gewin L, et al: Beta1 integrin expression by podocytes is required to maintain glomerular structural integrity. *Dev Biol* 316: 288–301, 2008

58. Kadrmas JL, Beckerle MC: The LIM domain: From the cytoskeleton to the nucleus. *Nat Rev Mol Cell Biol* 5: 920–931, 2004

AFFILIATIONS

[1]Division of Nephrology, Department of Medicine, Icahn School of Medicine at Mount Sinai, New York, New York

[2]Department of Mechanical Engineering, Columbia University, New York, New York

[3]Department of Pathology, Icahn School of Medicine at Mount Sinai, New York, New York

[4]Department of Neuroscience, Icahn School of Medicine at Mount Sinai, New York, New York

[5]Department of Nephrology, Children's Hospital of Nanjing Medical University, Nanjing, China

[6]Department of Microbiology, Biochemistry and Molecular Genetics, Rutgers University–New Jersey Medical School, Newark, New Jersey

[7]Department of Pharmacological Sciences, Icahn School of Medicine at Mount Sinai, New York, New York